

FABRICATION AND AEROELASTIC ANALYSIS OF SILICONE MEMBRANE MICRO
AIR VEHICLE WINGS

By

ALBERT Y. LIN

A THESIS PRESENTED TO THE GRADUATE SCHOOL
OF THE UNIVERSITY OF FLORIDA IN PARTIAL FULFILLMENT
OF THE REQUIREMENTS FOR THE DEGREE OF
MASTER OF SCIENCE

UNIVERSITY OF FLORIDA

2009

© 2009 Albert Y. Lin

To Mom

ACKNOWLEDGMENTS

I would like to take this opportunity to thank everyone who has contributed to my academics, research, and life throughout graduate school.

Yaakov Abudaram, for your camaraderie throughout the MAV Lab, wind tunnel, and graduate school in general.

Mulugeta Haile, for your friendship and help with many lab experiments.

Vijay Jagdale, for teaching me the particulars of the VIC system.

Kyuhoo Lee, for your passion and talent in aircraft design.

Dr. Bret Stanford, for teaching me the intricacies of the wind tunnel and your wealth of academic knowledge. Thank you for taking time to answer my questions.

Pin Wu, for your conversations and generosity in sharing your laboratory.

My family, for your love and constant support.

Kim, Champ, Rhyley, and Lt. Dan, for your love and many happy memories.

I owe many thanks to Dr. Peter Ifju, for giving me so many opportunities to succeed. You are a patient, enthusiastic, and talented teacher and I enjoyed my time working with you. Thank you for everything that you have done for me.

TABLE OF CONTENTS

	<u>page</u>
ACKNOWLEDGMENTS	4
LIST OF TABLES	7
LIST OF FIGURES	8
LIST OF ABBREVIATIONS	11
ABSTRACT	12
CHAPTER	
1 INTRODUCTION	13
Motivation	13
Objectives	15
Outline	15
2 LITERATURE REVIEW	16
3 EXPERIMENTAL DATA SYSTEMS	20
Closed-Loop Wind Tunnel	20
Visual Image Correlation	21
4 SILICONE MEMBRANE FABRICATION	23
Baseline Airfoil	23
Design Process	23
Step One: Construct Composite Airframe	24
Step Two: Mix Silicone Compound	25
Step Three: Apply Silicone Compound	26
Step Four: Apply Vacuum Pressure	26
Step Five: VIC Preparation	29
5 AEROELASTIC ANALYSIS	30
VIC Analysis	30
Membrane Pre-Tension Validation	30
Topology Optimization Design Comparison	35
Aerodynamic Data	41
6 RELATED CONCEPTS	46

7	CONCLUSION.....	47
	Conclusion.....	47
	Future Work.....	47
APPENDIX		
A	EXPERIMENTAL OUT-OF-PLANE DISPLACEMENTS FOR BASELINE AND TOPOLOGY OPTIMIZED WING DESIGNS	49
B	NUMERICAL OUT-OF-PLANE DISPLACEMENT MODELS FOR BASELINE AND TOPOLOGY OPTIMIZED WING DESIGNS, COURTESY OF STANFORD [4].....	60
	LIST OF REFERENCES.....	66
	BIOGRAPHICAL SKETCH	68

LIST OF TABLES

<u>Table</u>		<u>page</u>
2-1	Mechanical properties of silicone rubber	19
4-1	Properties of Dragon Skin®.....	25
5-1	Maximum out-of-plane displacements and locations, PR wing	30
5-2	Maximum membrane displacements, PR wing.....	35
5-3	Maximum out-of-plane displacement comparisons, $\alpha = 12^\circ$	40

LIST OF FIGURES

<u>Figure</u>	<u>page</u>
1-1 Erosion of latex at the bonding surfaces of BR wing after 60 days.	14
2-1 Cornell University bat wing design with nylon fabric affixed to carbon fiber skeletal fingers [8].	17
2-2 Cornell University bat wing design with thin silicone sheets glued to a steel wire skeletal frame [8].	18
3-1 Schematic of the experimental test section.	20
3-2 Random speckling pattern for VIC analysis.	21
3-3 VIC system arrangement above wind tunnel test section.	22
3-4 VIC cameras collect images through wind tunnel ceiling optical glass access.	22
4-1 Types of wings constructed using the baseline airfoil.	23
4-2 Cured carbon fiber TOP wing structure placed onto wing tool for membrane preparation.	24
4-3 Pigmented liquid silicone compound applied to TOP wing.	26
4-4 Wing mold containing composite frame and silicone compound under vacuum pressure.	27
4-5 Creating a reverse imprint for the cavity mold using slow-curing epoxy.	28
4-6 Compression mold assembly for the baseline MAV wing.	28
4-7 Compression mold assembly under 30 mm Hg vacuum pressure.	29
5-1 Experimental out-of-plane displacement contour, silicone membrane PR wing, $\alpha = 12^\circ$ (refer Appendix A).	31
5-2 Normalized out-of-plane displacement (w/c), silicone membrane PR wing, $\alpha = 12^\circ$	31
5-3 Out-of-plane displacement comparison of silicone membrane (top) and latex membrane PR (bottom), $\alpha = 12^\circ$	32
5-4 Normalized out-of-plane displacement comparison, PR membrane, $\alpha = 12^\circ$	33
5-5 Out-of-plane displacement comparison, regular (top) and viscosity-reduced (bottom) silicone membrane PR wing, $\alpha = 12^\circ$	34

5-6	Out-of-plane displacements along $2y/b = 0.58$ of various PR membranes, $\alpha = 12^\circ$	35
5-7	Numerical (top) and experimental (bottom) out-of-plane displacements for baseline and topology optimized designs, $\alpha = 12^\circ$	36
5-8	Experimental (left) and numerical (right) out-of-plane displacements, rigid wing, $\alpha = 12^\circ$	37
5-9	Experimental (left) and numerical (right) out-of-plane displacements, PR wing, $\alpha = 12^\circ$	37
5-10	Experimental (left) and numerical (right) out-of-plane displacements, topology optimized wing for maximum lift ($TOP_{\max \text{ lift}}$), $\alpha = 12^\circ$	38
5-11	Experimental (left) and numerical (right) out-of-plane displacements, BR wing, $\alpha = 12^\circ$	38
5-12	Experimental (left) and numerical (right) out-of-plane displacements, topology optimized wing for minimum lift slope ($TOP_{\min \text{ lift slope}}$), $\alpha = 12^\circ$	39
5-13	Experimental (left) and numerical (right) out-of-plane displacements, $\delta = 1.0$ optimization wing for minimum lift slope ($TOP_{\delta=1}$), $\alpha = 12^\circ$	39
5-14	Baseline and TOP design shapes compared in Figures 5-8 through 5-13, respectively from left to right.....	40
5-15	Experimental (left) and numerical (right) out-of-plane displacements along $2y/b = 0.58$, baseline and topology designs, $\alpha = 12^\circ$	41
5-16	Experimental aerodynamic comparison, latex and silicone membrane PR wing, $v_\infty = 13 \text{ m/s}$, $\alpha = 0-30^\circ$	42
5-17	Experimental aerodynamic comparison, latex and silicone membrane BR wing, $v_\infty = 13 \text{ m/s}$, $\alpha = 0-30^\circ$	43
5-18	Experimental aerodynamic data for low-tensioned, latex membrane baseline and topology optimized designs by Stanford [4], $v_\infty = 13 \text{ m/s}$, $\alpha = 0-30^\circ$	44
5-19	Experimental aerodynamic data for uniform-tensioned, silicone membrane baseline and topology optimized designs (from Figure 5-17), $v_\infty = 13 \text{ m/s}$, $\alpha = 0-30^\circ$	45
6-1	Fabrication of 24-inch BR piezoelectric concept wing membrane with pigmented liquid silicone compound.....	46
6-2	24-inch BR piezoelectric concept wing.....	46
A-1	Experimental out-of-plane displacement contour, rigid wing, $\alpha = 12^\circ$	49

A-2	Experimental out-of-plane displacement contour, silicone membrane PR wing, $\alpha = 12^\circ$	50
A-3	Experimental out-of-plane displacement contour, viscosity-reduced silicone membrane PR wing, $\alpha = 12^\circ$	51
A-4	Experimental out-of-plane displacement contour, latex membrane PR wing, $\alpha = 12^\circ$...	52
A-5	Experimental out-of-plane displacement contour, silicone membrane BR wing, $\alpha = 12^\circ$	53
A-6	Experimental out-of-plane displacement contour, silicone membrane TOP wing optimized for maximum lift ($TOP_{\max \text{ lift}}$), $\alpha = 12^\circ$ (refer [4], Figure 7-10).....	54
A-7	Experimental out-of-plane displacement contour, silicone membrane TOP wing optimized for minimum lift slope ($TOP_{\min \text{ lift slope}}$), $\alpha = 12^\circ$ (refer [4], Figure 7-10).....	55
A-8	Experimental out-of-plane displacement contour, silicone membrane TOP wing optimized for minimum C_L ($TOP_{\min C_L}$), $\alpha = 12^\circ$ (refer [4], Figure 7-15).....	56
A-9	Experimental out-of-plane displacement contour, silicone membrane TOP wing optimized for minimum C_D ($TOP_{\min C_D}$), $\alpha = 12^\circ$ (refer [4], Figure 7-15).....	57
A-10	Experimental out-of-plane displacement contour, silicone membrane TOP wing optimized for minimum C_m ($TOP_{\min C_m}$), $\alpha = 12^\circ$ (refer [4], Figure 7-15).	58
A-11	Experimental out-of-plane displacement contour, silicone membrane TOP wing, single-objective ($\delta = 1.0$) optimized for minimum lift slope ($TOP_{\delta=1}$), $\alpha = 12^\circ$ (refer [4], Figure 7-18).....	59
B-1	Numerical out-of-plane displacement model, rigid wing, $\alpha = 12^\circ$	60
B-2	Numerical out-of-plane displacement model, PR wing, $\alpha = 12^\circ$	61
B-3	Numerical out-of-plane displacement model, silicone membrane TOP wing optimized for maximum lift ($TOP_{\max \text{ lift}}$), $\alpha = 12^\circ$ (refer [4], Figure 7-10).	62
B-4	Numerical out-of-plane displacement model, BR wing, $\alpha = 12^\circ$	63
B-5	Numerical out-of-plane displacement model, silicone membrane TOP wing optimized for minimum lift slope ($TOP_{\min \text{ lift slope}}$), $\alpha = 12^\circ$ (refer [4], Figure 7-10).....	64
B-6	Numerical out-of-plane displacement model, silicone membrane TOP wing, single-objective ($\delta = 1.0$) optimized for minimum lift slope ($TOP_{\delta=1}$), $\alpha = 12^\circ$ (refer [4], Figure 7-18).....	65

LIST OF ABBREVIATIONS

Al	aluminum
BR	batten reinforced
C	Celsius
cps	centipoises
Hg	mercury
hrs	hours
in	inch
KOH	potassium hydroxide
lb	pound
m	meter(s)
MAV	micro air vehicle
MEMS	microelectromechanical systems
mm	millimeter
N	Newton
parylene-C	poly-monochloro-para-xylylene
pli	pounds per linear inch
PR	perimeter reinforced
RTV	room temperature vulcanizing
s	second
Ti	titanium
TOP	topology optimized
UAV	unmanned aerial vehicle
v_{∞}	freestream velocity
VIC	visual image correlation

Abstract of Thesis Presented to the Graduate School
of the University of Florida in Partial Fulfillment of the
Requirements for the Degree of Master of Science

FABRICATION AND AEROELASTIC ANALYSIS OF SILICONE MEMBRANE MICRO
AIR VEHICLE WINGS

By

Albert Y. Lin

December 2009

Chair: Peter Ifju

Major: Aerospace Engineering

Flexible wing micro air vehicles (MAVs) have been developed at the University of Florida to improve adverse flying conditions. Typically, such MAVs display low Reynolds numbers and low aspect ratios. Current designs use elastic membranes bonded to a carbon fiber wing structure. A variety of materials are functional as integrated membranes, such as latex and polyester film. However, two design issues are presented with existing manufacturing procedures. First, membrane materials lack robustness as they are vulnerable to rupture, environmental conditions, and prolonged shelf-life. Second, uniform membrane pre-tension is essentially unattainable by current procedures, causing disparities which can significantly alter flight dynamics and create aeroelastic instabilities. A technique is developed which uses high performance platinum-cure silicone rubber to fabricate wing membranes exhibiting uniform pre-tension. Silicone rubber displays durability, high physical properties, and robustness in its function as an integrated MAV membrane. Visual image correlation is performed to validate silicone membrane displacements and pre-tensions of selected wing designs, as well as comparisons to latex membrane counterparts. Experimental data, including aerodynamic analysis, is further examined for aeroelastic topology optimized wings and compared with numerical models.

CHAPTER 1 INTRODUCTION

Motivation

Numerous micro air vehicles (MAVs) designed at the University of Florida are based on flexible wing structures, due to fixed-wing aerodynamic challenges resulting from low Reynolds numbers (10^4 - 10^5) [1]. The basic design is composed of a composite laminate frame with an affixed flexible membrane skin, which allows passive shape adaption [2]. Latex, mylar/polyester film, ecorex, and nylon are typical materials used as membrane skins, with latex being the most common. Perimeter reinforced (PR) wings have unconstrained interior membranes, bonded to a rigid composite perimeter. PR membranes allow for camber adaptation to varying flight conditions and wind gusts, translating load distributions on the wing which increases C_L and decreases $C_{m\alpha}$ [3]. Batten reinforced (BR) wings are designed with uni-directional strips of carbon fiber parallel to the chord line, extending from the leading edge to an unconstrained trailing edge. The battens are adhered to the membrane skin, much like a bat wing, to provide flight load alleviation. Topology optimized (TOP) wings contain composite laminate distributions positioned in specific locations on the membrane. These shapes and locations correspond to specifically optimized aerodynamic functions [4].

Latex of minimal thickness (on the order of 0.12 mm) is typically used because of billowing effects which aid in load distribution. After fabricating numerous latex membrane wings, two significant design issues were observed. Latex membranes are not robust. They are not durable and are susceptible to tearing, punctures, and erosion due to heat, UV, and chemical agents. Figure 1-1 shows erosion of a latex membrane in contact with spray glue adhesive after 60 days. Degradation at the bonding points of the membrane inhibits flight performance consistency and is detrimental to shelf life.



Figure 1-1. Erosion of latex at the bonding surfaces of BR wing after 60 days.

Second, uniform membrane per-tension is difficult to achieve and cannot be controlled by existing manufacturing methods. Adaptive cambering membranes differing in pre-tension could cause instabilities, greatly affecting flight dynamics of the aircraft. Consider a PR wing designed for high lift, high drag which is manufactured with too much tension on one membrane. The higher pre-tensioned membrane would require less drag, having more streamline shape. The lower pre-tensioned membrane would have a larger deformation, thus higher drag. This scenario could cause longitudinal and lateral instability of the wing, creating an adverse situation which defeats the purpose of the intended design.

The purpose of this research is to develop a superior flexible membrane for incorporation onto composite MAV wings. This requires a fabrication process to address the aforementioned concerns, and silicone rubber will be introduced as the ideal material for this process.

Objectives

1. Develop a method to fabricate MAV wing membranes using platinum-cure silicone rubber.
2. Develop a method to create silicone membranes with uniform pre-tension.
3. Experimental validation of uniform membrane pre-tension.
4. Experimental comparison of latex and silicone membrane wings.
5. Experimental comparison and validation of topology optimized designs.
6. Fabricate conceptual wing designs using silicone rubber as the integration platform.

Outline

Chapter 2 is a literature review of bio-inspired designs, a silicone bat wing fabrication process developed at Cornell University, and advantages of silicone rubber as a flexible MAV membrane.

Chapter 3 classifies experimental apparatus and data analysis procedures. This involves the visual image correlation system and closed-loop low-speed wind tunnel.

Chapter 4 details the silicone membrane fabrication process. A step-by-step method is provided for co-curing room temperature vulcanizing silicone rubber to carbon fiber structures. This chapter also provides visual image correlation preparation.

Chapter 5 analyzes experimental aeroelastic data. The PR design is used to validate pre-tension uniformity of silicone membranes. A comparison is made between silicone membrane wings and their latex membrane counterparts. Selected optimal topology wing designs are evaluated and compared to numerical models.

Chapter 6 presents concepts related to bio-inspired wing designs and control surface integration with silicone membranes.

CHAPTER 2 LITERATURE REVIEW

Currently, no manufacturing process exists for co-curing silicone rubber onto composite MAV wings as functional flexible membranes. Growing research interests in bio-inspired, skeletal-based designs have sparked intriguing innovations pursuing biological qualities and morphing features. Pornsin-sirirak et al. [5] present a MEMS-based wing technology which uses a titanium-alloy metal (Ti-6Al-4V) wingframe with a poly-monochloro-para-xylylene (parylene-C) membrane. Target MEMS wings include bio-inspired designs such as beetles, dragonflies, butterflies, and bats. Early efforts utilized silicon nitride pattern depositions and potassium hydroxide (KOH) etching to create wingframes. However, silicon wingframes were too fragile and abandoned in favor of the titanium-alloy metal.

Thin, compliant skin membranes unique to flying and gliding animals (bats, flying squirrels, sugar gliders, etc.) exhibit maneuverability and agility unseen in other flying species of comparable size [6]. Bat wing research has been conducted for piezoelectric actuation of joints [7], various flight characteristics to develop optimal shapes [8], and aerodynamic effects of membraned-wings [9]. Additionally, Waldman et al. [10] (Brown University) compares membrane airfoil behavior under aerodynamic loading with in vivo measurements of bat wings during flight. Bat membrane deformations are measured from recorded flight kinematics of a *Cynopterus brachyotis* in a wind tunnel, in which downstroke wing areas are observed to increase up to 100%.

Callahan and Garcia [11] discuss a bio-inspired bat wing fabrication method using a skeleton structure with various membrane materials incorporated at Cornell University. Initially, the skeleton was constructed with hollow carbon fiber rods, as it was light and strong enough to withstand pressure loads of an attached membrane. Due to instability at the joints and weight

concerns with epoxy adhesives, the skeletal design was modified to steel rods with composite fibers wrapped tightly around adjoining sections. Three membrane materials were tested: nylon fabric, spandex fabric, and silicone sheets. Nylon and spandex fabrics were cut to desired wing shapes and fused to the skeleton joints with epoxy. Skeletal fingers, shown in Figure 2-1, were sewn securely to fabric material with needle and thread. Even so, thin silicone sheets (also cut to desired wing shapes) were determined to be the most appropriate membrane material because it was sturdy, flexible, and stable under slight loading conditions. It also had a similar feel to live bats and was more rugged than latex. The main issue, however, was that silicone bonds only to itself. Wing assembly was therefore accomplished with a silicone-based glue to adhere the thin silicone sheets to the steel wire frame (Figure 2-2). Chapter 4 introduces an alternative silicone membrane fabrication method to [11]. Room temperature vulcanizing (RTV) silicone rubber as a liquid compound is used to fabricate membranes instead of thin silicone sheets. The compound is co-cured onto carbon fiber wing structures, hence eliminating the use of silicone-based adhesives.



Figure 2-1. Cornell University bat wing design with nylon fabric affixed to carbon fiber skeletal fingers [8].



Figure 2-2. Cornell University bat wing design with thin silicone sheets glued to a steel wire skeletal frame [8].

Silicone rubber is an ideal membrane material because of its extremely elastic nature and favorable material properties. Normally, the compound requires heat to vulcanize. In this work, however, a high-purity pourable silicone rubber is used. It is a platinum-cured, RTV compound having liquid consistency [12]. The silicone compound is supplied in two parts which are mixed together, one of which contains the platinum catalyst. Additive agents such as pigments and viscosity reducers are also available if desired. The pot life is approximately 20-40 minutes. Typical mechanical properties of silicone rubber are listed in Table 2-1. Silicone rubber is an ideal material for UAV membranes because of these characteristics:

- Good resistance to extreme temperatures
- High resistance to ozone, radiation, and ageing factors
- Hydrophobic properties
- Efficient electrical insulation
- Exhibits flame retardant features
- Highly inert material

It is superior to other elastomers with regard to thermal properties. At extreme temperatures, elasticity is sustained to -60°C and exhibits a flash point of 750°C . Recently, silicone rubber was even observed to have self-healing traits, as the material was capable of recovering almost all of its original tear strength [13].

Table 2-1. Mechanical properties of silicone rubber

Property	Quantity
Hardness, Shore A	10-90
Tensile strength	11 N/mm ²
Elongation at break	100-1100%
Max. temperature	+300°C
Min. temperature	-120°C

CHAPTER 3 EXPERIMENTAL DATA SYSTEMS

Closed-Loop Wind Tunnel

Aerodynamic analysis is conducted in a closed-loop wind tunnel manufactured by Engineering Laboratory Design, Inc (model 407B). A two-stage axial fan directs horizontal airflow up to a limit of 45 m/s through a 33-inch test section. Force and moment measurements are made by an internal AEROLAB strain gage sting balance, capable of six degrees-of-freedom and measuring loads on the order of 0.01 N [14]. It is supported by a U-shaped model arm connected to a motorized motion controller, rotating pitch rates at approximately 1°/s. Wing models are bolted to the tip of the sting balance with a bracket mount, using an inclinometer to adjust model and balance offsets. Aerodynamic loads are collected at 13 m/s with an α -sweep of 0-30°. Out-of-plane displacement data is gathered at 13 m/s, $\alpha = 12^\circ$.

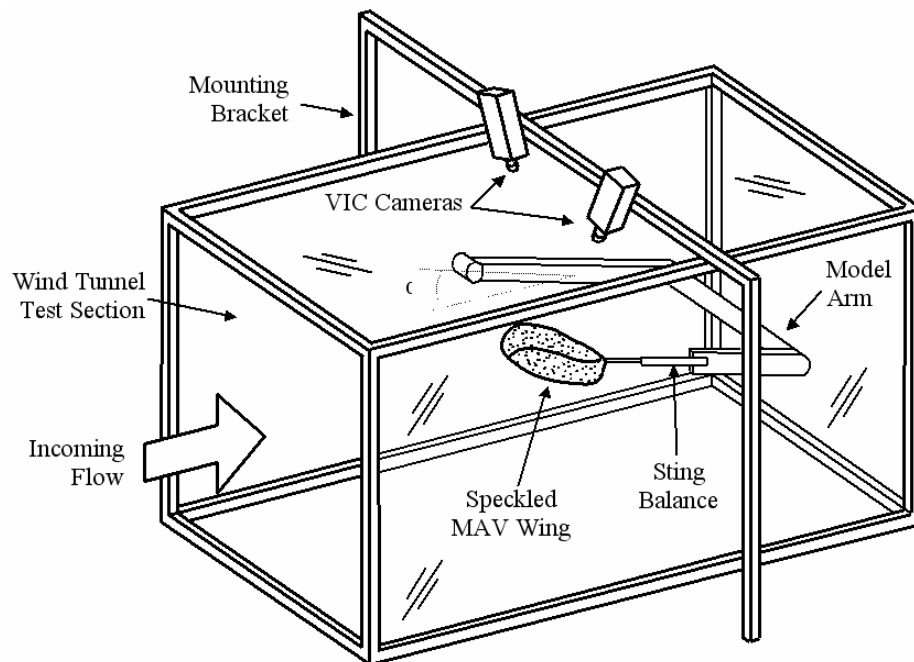


Figure 3-1. Schematic of the experimental test section.

Visual Image Correlation

The visual image correlation (VIC) system is a non-intrusive method of obtaining full-field, 3-D deformation measurements. In this work, out-of-plane displacements are considered for wings experiencing induced airflow by the wind tunnel. For 3-D analysis, the optical arrangement includes two cameras to provide stereo imaging capabilities [15]. Test specimens are prepared with a random speckling pattern, which is recognized by system. Each speckle represents a unique shape and intensity, serving as ideal targets (Figure 3-2).



Figure 3-2. Random speckling pattern for VIC analysis.

Digital images are taken before and after the surface deformation. The correlation algorithm compares the intensity data from these two fields by mapping displacements, smoothing intensity data, and using a least squares correlation coefficient. Assuming target features are sufficient and calibration accurately performed, the displacement field can be established. Figures 3-3 and 3-4 show the VIC system setup in the wind tunnel test section.

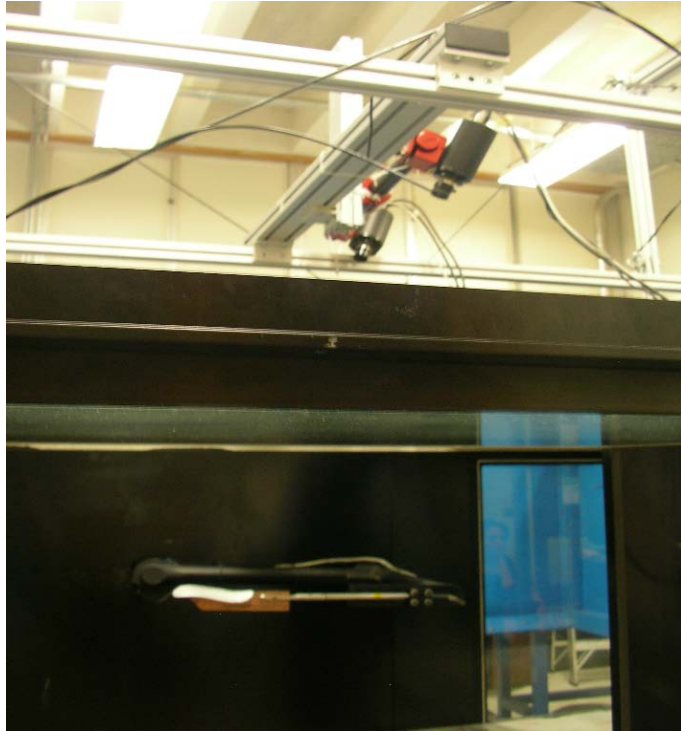


Figure 3-3. VIC system arrangement above wind tunnel test section.



Figure 3-4. VIC cameras collect images through wind tunnel ceiling optical glass access.

CHAPTER 4 SILICONE MEMBRANE FABRICATION

Baseline Airfoil

Baseline airfoil characteristics used in this work are:

- 152 mm wingspan
- 124 mm root chord
- 1.25 aspect ratio
- 6.8% camber at the root (located at $x/c = 0.22$)
- -1.4% reflex at the root (located at $x/c = 0.86$)
- 7° dihedral (between $2y/b = 0.4$ and the wingtip)
- 7° geometric twist (nose up) at the wingtips

Figure 4-1 shows the different types of wings constructed using this airfoil: PR, BR, and TOP wings. Wings are constructed with two layers of carbon fiber (3000 fiber/tow, pre-impregnated with thermoset epoxy) in a plain weave, bi-directional ($0^\circ/90^\circ$) orientation. The leading edge includes an extra layer of carbon fiber, adding stiffness to offset torsion. The battens of the BR wings consist of two layers of uni-directional carbon fiber. Laminate shells of the TOP wings are made from one layer of bi-directional carbon fiber.



Figure 4-1. Types of wings constructed using the baseline airfoil. A) PR wing. B) BR wing. C) TOP wing.

Design Process

A series of techniques were developed for fabricating silicone membrane wings with uniform membrane thickness and pre-tension.

Step One: Construct Composite Airframe

The first step is to construct the carbon fiber frame using standard manufacturing, vacuum-bagging, and curing procedures.



Figure 4-2. Cured carbon fiber TOP wing structure placed onto wing tool for membrane preparation.

Initially, silicone was co-cured with the carbon fiber layup during the curing cycle. This was done under the premise that interaction with the thermoset epoxy during the curing cycle would promote adhesion to carbon fiber. Although the membrane successfully adhered to the wing, the carbon fiber layup occasionally warped during distribution of the pre-vulcanized silicone rubber when vacuum pressure was applied. This occurred most often in TOP wing fabrication, as the silicone compound would shift laminate shells from their desired locations.

The process was repeated with a cured carbon fiber frame, yielding these observations:

1. Under vacuum pressure, silicone adhesion strength to carbon fiber is indistinguishable between the co-cured and cured process.
2. Under vacuum pressure, silicone adhesion to a cured carbon fiber frame is not temperature dependent.

- Both methods are successful, but it is much easier to fabricate silicone membrane wings using a cured carbon fiber frame.

An increase in temperature accelerated the vulcanization rate of the silicone compound, but did not affect the bonding strength to carbon fiber. From a manufacturing standpoint, the best approach is to cure the carbon fiber structure first. It eliminates structural warping and prevents laminate shifting of TOP wings. However, future work is suggested to measure the adhesion strength between RTV and temperature-accelerated silicone.

Step Two: Mix Silicone Compound

The next step is to mix the silicone compound. Once the components are mixed, the liquid silicone is centrifuged (approximately 3 minutes) to eliminate air bubbles from the solution. The silicone rubber used is called Dragon Skin®, manufactured by Smooth-On, Inc. It is a two-component, platinum curing silicone elastomer composed of polyorganosiloxanes, amorphous silica, and platinum-siloxane complex. This material is extremely flexible and yields a high tear strength.

Table 4-1. Properties of Dragon Skin®

Property	Quantity
Elongation at break	1000%
Mixed viscosity	23000 cps
Shore A hardness	10
Tear strength	102 pli
Weight	25.8 in ³ /lb
Demold time	5 hrs

Silicone additives may be applied to assist with membrane thickness and enhance VIC analysis. A thinning agent (SilcThin®) was used to reduce the viscosity of the mixture to improve workability and prolong pot life. However, this additive does reduce material strength. The maximum amount allowed is 7.5% of the total mixture weight.

Step Three: Apply Silicone Compound

Once air bubbles are removed, the silicone is applied to the wing tool. For releasing purposes, a layer of Teflon film is affixed to the wing tool with a thin coat of spray glue. It is essential to keep the wing tool smooth and free of defects as this surface directly translates to the surface of the membrane. At this point, the carbon fiber frame is placed onto the wing tool and silicone is poured onto the proper locations.



Figure 4-3. Pigmented liquid silicone compound applied to TOP wing.

Step Four: Apply Vacuum Pressure

The mold is placed in a vacuum bag under a suction pressure of 30 mm Hg [16]. Initially, the silicone was smoothed out by hand and rubber rollers through the vacuum bag (Figure 4-4). This method created two major setbacks. First, warping and shifting of the wing structure (expressed in Step One) occurred, primarily in un-cured carbon fiber frames and TOP wings. Second, the cured silicone membrane did not have consistent thickness. The thickness disparity

was noticeable by eye, especially at the maximum wing camber where the silicone accumulated. There were also regions of the membrane which were extremely thin due to the inconsistent smoothing process.



Figure 4-4. Wing mold containing composite frame and silicone compound under vacuum pressure.

Creating a membrane of uniform thickness is critical because of the adaptive cambering and load-alleviating nature of these wing designs. In addition, unnecessary weight is added to the wing due to the excess silicone. Manufacturing a compression mold for the wing was the most consistent way to fabricate silicone membranes of uniform thickness. This was done by using the original mold and generating a cavity mold using a slow-curing epoxy. Figure 4-5 shows the epoxy being cured in the wing tool, creating a reverse imprint for the cavity mold. The mold was bagged and put under vacuum pressure to create a smooth surface. Multiple coats of Frekote (mold release agent) was applied to the surface before adding epoxy. Screws were placed on either side to aid in removing the cured epoxy.



Figure 4-5. Creating a reverse imprint for the cavity mold using slow-curing epoxy.

Holes were drilled around the edge to create a vented cavity mold. This allows for maximum amount of air to be vacuumed out by the pump creating a smooth, thin membrane. For releasing purposes, a layer of Teflon is affixed to the cavity mold with a thin mist of spray adhesive. The composite frame and silicone compound is then sandwiched between the compression mold (Figure 4-6) before being placed under vacuum pressure (Figure 4-7). It is important not to use too much spray adhesive because accumulation between the Teflon and mold surface will create defects in the finished membrane.

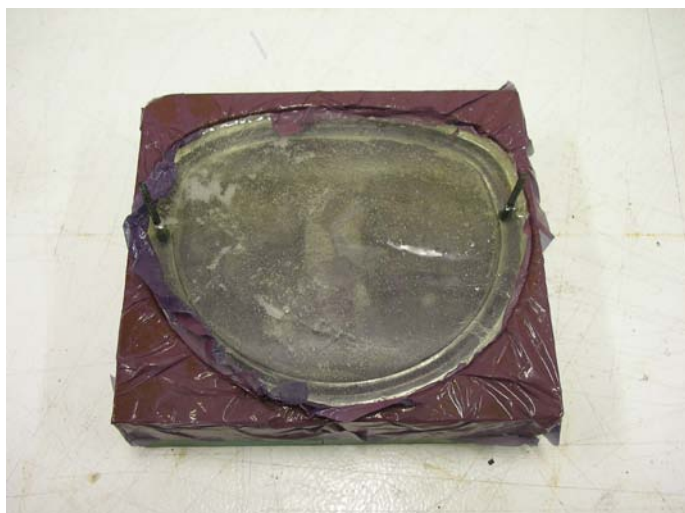


Figure 4-6. Compression mold assembly for the baseline MAV wing.



Figure 4-7. Compression mold assembly under 30 mm Hg vacuum pressure.

Step Five: VIC Preparation

This step is provided if VIC analysis is desired. White pigment can be added to the silicone compound to enhance VIC pattern recognition. Cured pigmented membranes have a glossy finish nonetheless, so a very light coat of flat white paint is applied to the wing before the speckling pattern. Although paint does not adhere well to silicone, a minute coat to dull the glossy features is sufficient. A random speckling pattern is sprayed onto the wing with flat black paint. The nozzle of the spray paint was enlarged to create larger drops for the pattern instead of mist. Speckling patterns did not fail during wind tunnel testing under an applied load.

CHAPTER 5 AEROELASTIC ANALYSIS

VIC Analysis

VIC analysis was conducted on baseline and topology optimized wing designs in the wind tunnel at $v_\infty = 13$ m/s and $\alpha = 12^\circ$. Objectives are to:

- Validate uniform pre-tension of silicone membranes
- Compare latex and silicone membrane designs
- Observe the effects of reduced-viscosity silicone
- Compare experimental results with numerical models of topology optimized designs

Membrane Pre-Tension Validation

The PR wing was used as the baseline for validating uniform membrane tension. Figure 5-1 shows the symmetry of out-of-plane displacements across both membranes. Inflation occurs at the consistent locations along spanwise sections. Maximum out-of-plane displacement is 6.45 mm, measured at $2y/b = -0.70$ for the left membrane and 6.48 mm, measured at $2y/b = 0.68$ for the right membrane (Figure 5-2). Figure 5-3 compares the silicone membrane PR wing to its latex membrane counterpart. The same PR wingframe was used to construct both wings. Latex membranes were adhered with low-tension to promote maximum inflation for this comparison. Also, uniform pre-tension was attempted when adhering the latex membranes. Although maximum out-of-plane displacements do not differ by much (Figure 5-4), Figure 5-3 is evidence that the latex membrane vastly underachieves in its attempt at membrane pre-tension uniformity. The contour also reveals inconsistent and decreased inflation surface area for the latex membranes. Maximum out-of-plane displacements are shown in Table 5-1.

Table 5-1. Maximum out-of-plane displacements and locations, PR wing

Membrane	w [mm]	Location (2y/b)
Silicone, left	6.45	-0.70
Silicone, right	6.48	0.68
Latex, left	6.43	-0.58
Latex, right	5.76	0.68

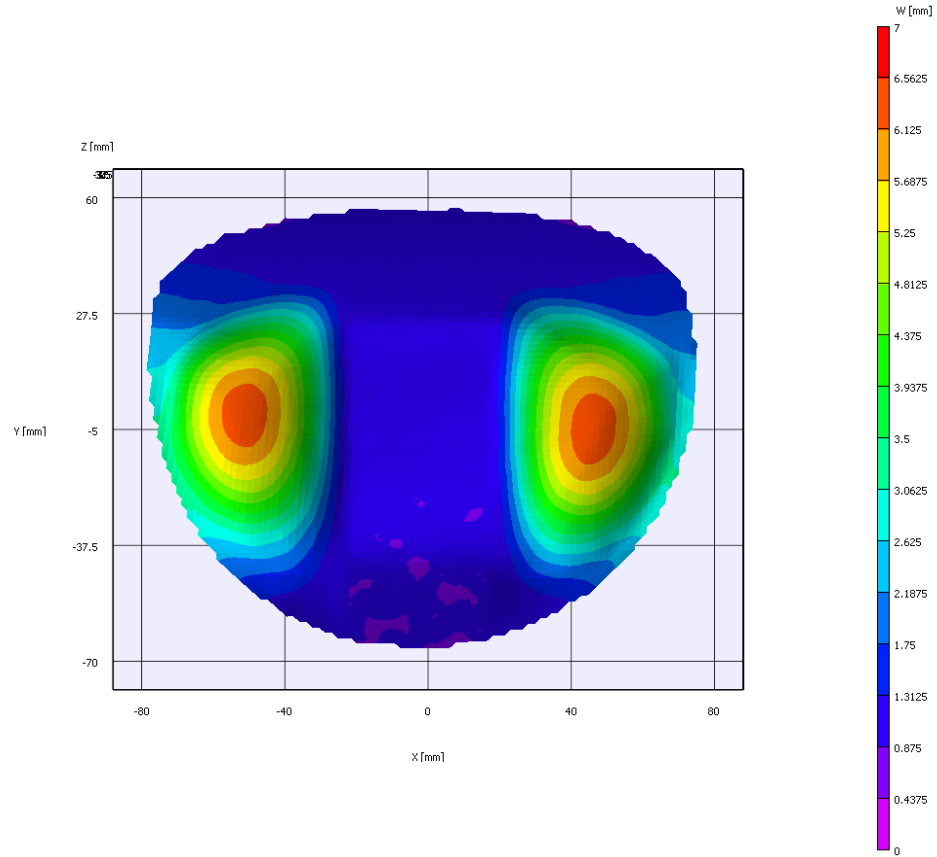


Figure 5-1. Experimental out-of-plane displacement contour, silicone membrane PR wing, $\alpha = 12^\circ$ (refer Appendix A).

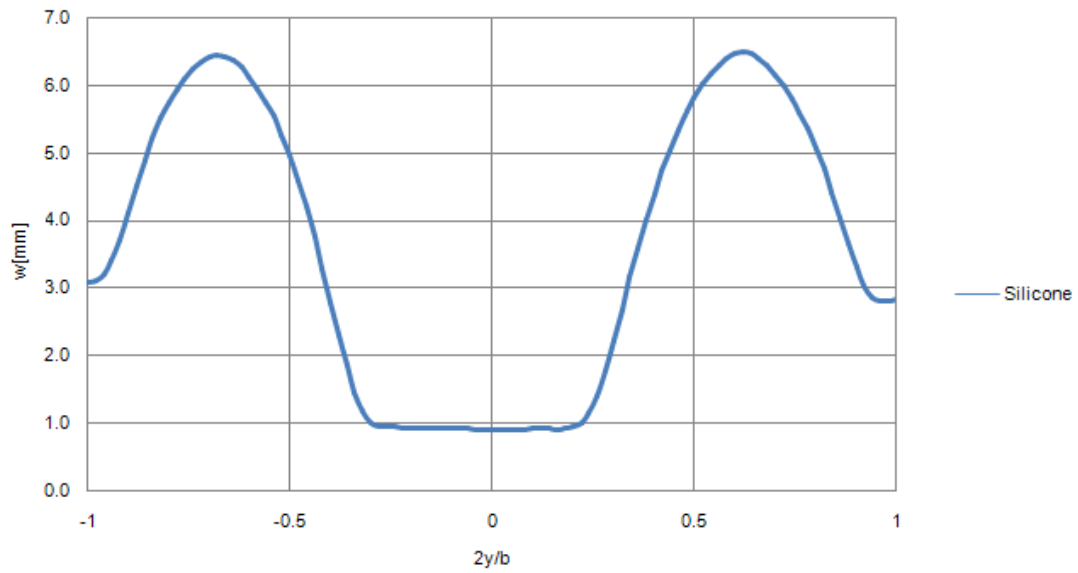


Figure 5-2. Normalized out-of-plane displacement (w/c), silicone membrane PR wing, $\alpha = 12^\circ$.

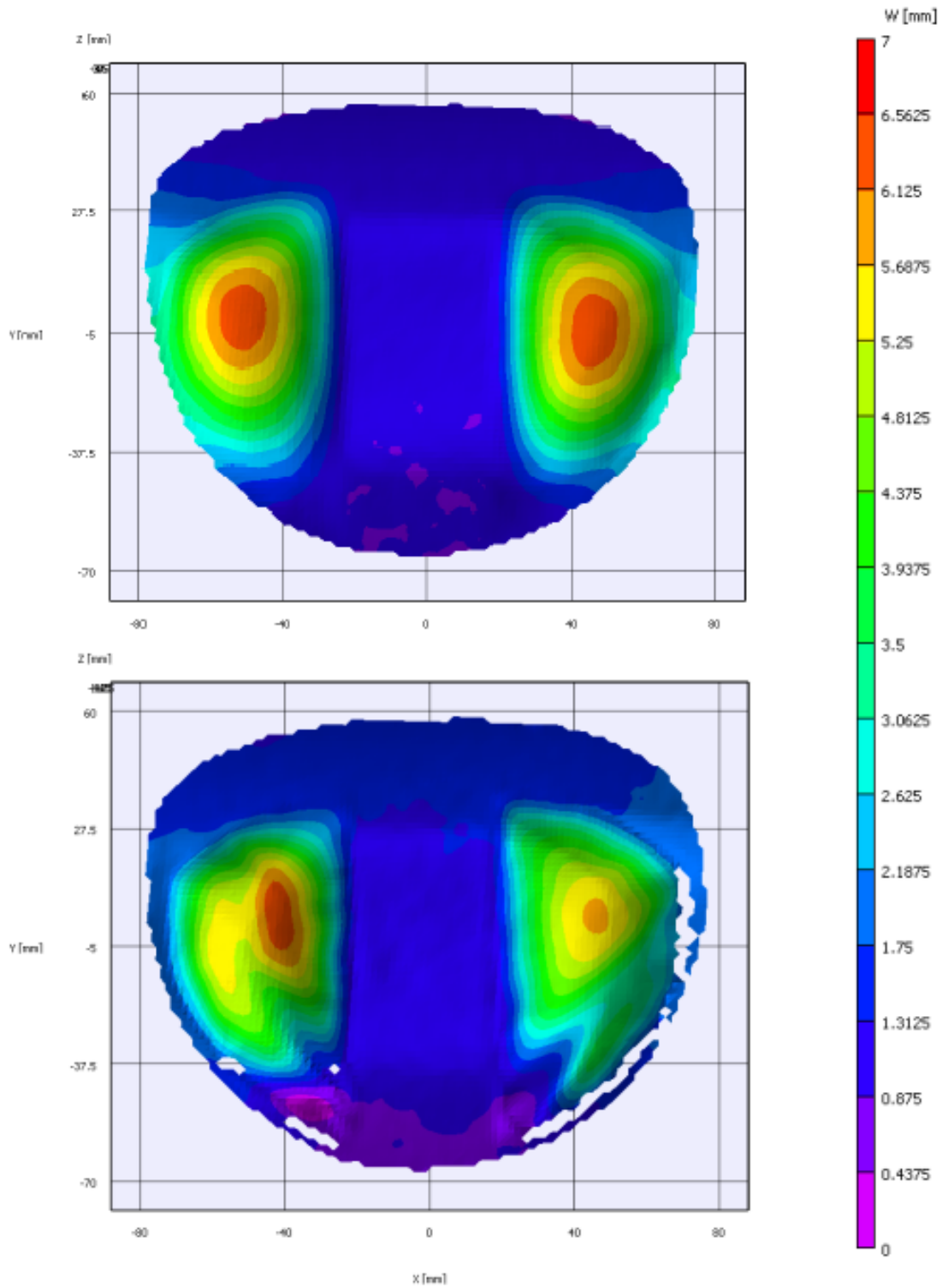


Figure 5-3. Out-of-plane displacement comparison of silicone membrane (top) and latex membrane PR (bottom), $\alpha = 12^\circ$.

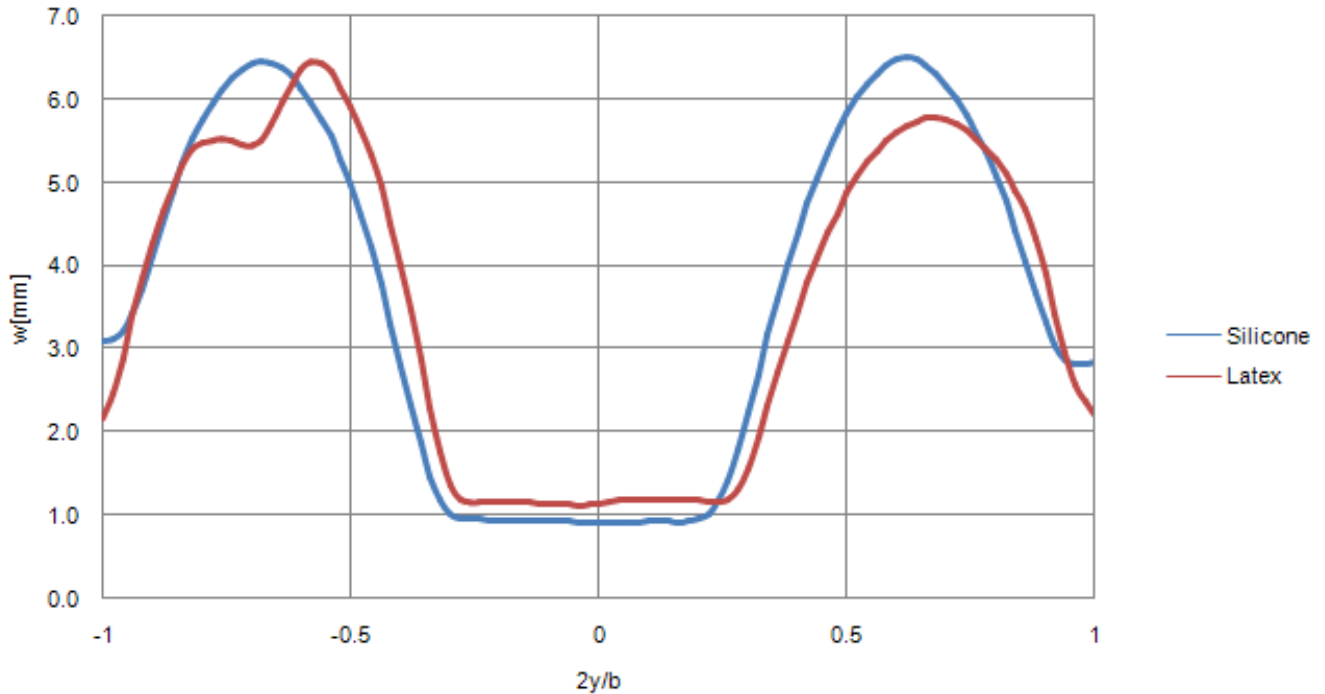


Figure 5-4. Normalized out-of-plane displacement comparison, PR membrane, $\alpha = 12^\circ$.

Now that uniform pre-tension across both membranes can be achieved, is it possible to control it? The ability to control membrane pre-tension would allow flexible wings to be extremely versatile. Low-tensioned membranes could be used for applications requiring increased lift and stability, while high-tensioned membranes could be used for reduced drag. A silicone thinning agent was tested to reduce material viscosity in hopes of creating thinner, lower-tensioned membranes. Figure 5-5 confirms increased billowing in viscosity-reduced membranes, as the membrane inflation is noticeably larger. The maximum out-of-plane displacement increase is 23% (1.42 mm) due to the addition of the viscosity-reducing agent and 31% (1.80 mm) compared to the latex membrane. Figure 5-6 depicts not only a higher peak, but also an increase in inflation surface area. Displacements along the spanwise section $2y/b = 0.58$ have maximum values shown in Table 5-2.

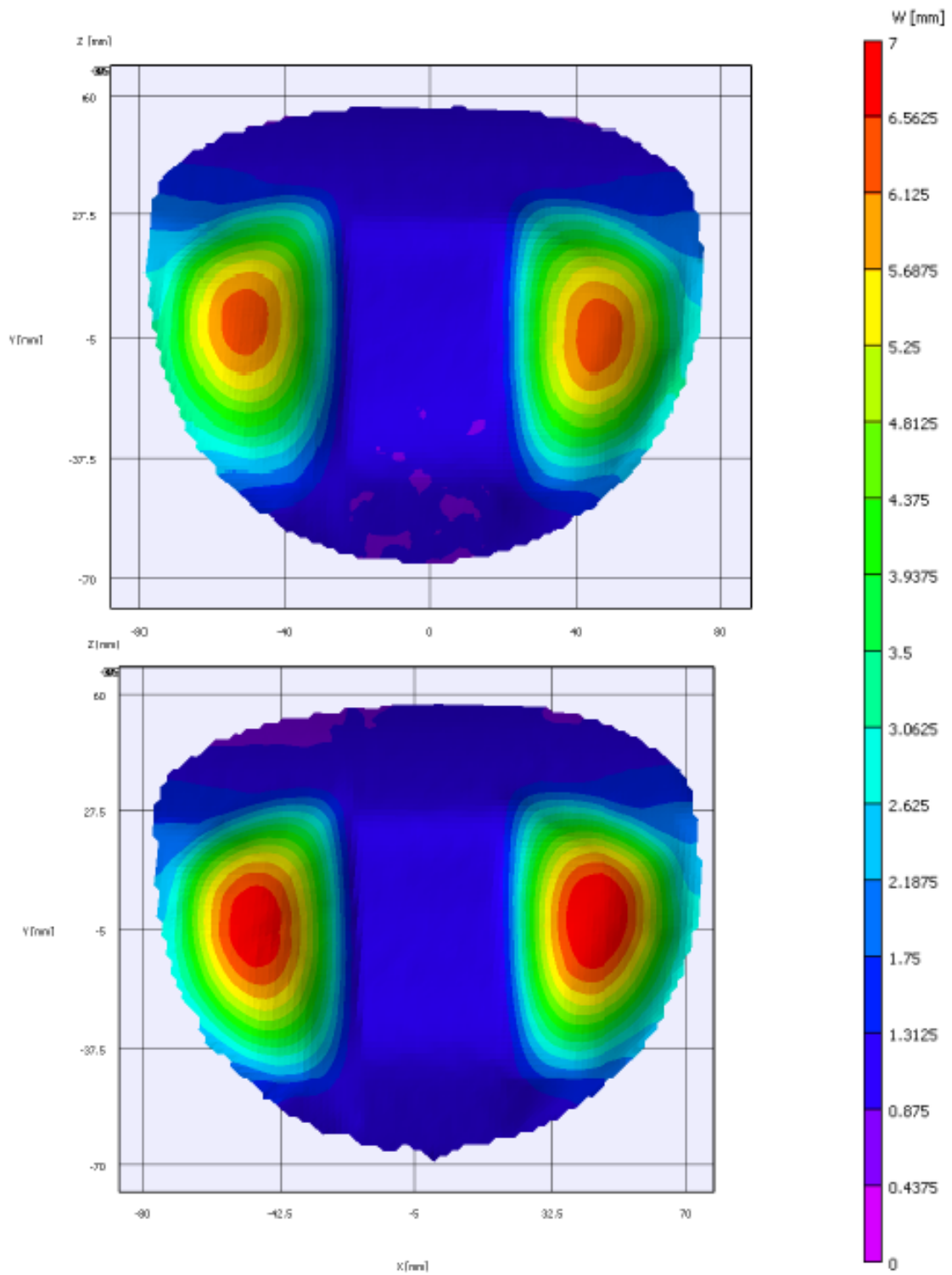


Figure 5-5. Out-of-plane displacement comparison, regular (top) and viscosity-reduced (bottom) silicone membrane PR wing, $\alpha = 12^\circ$.

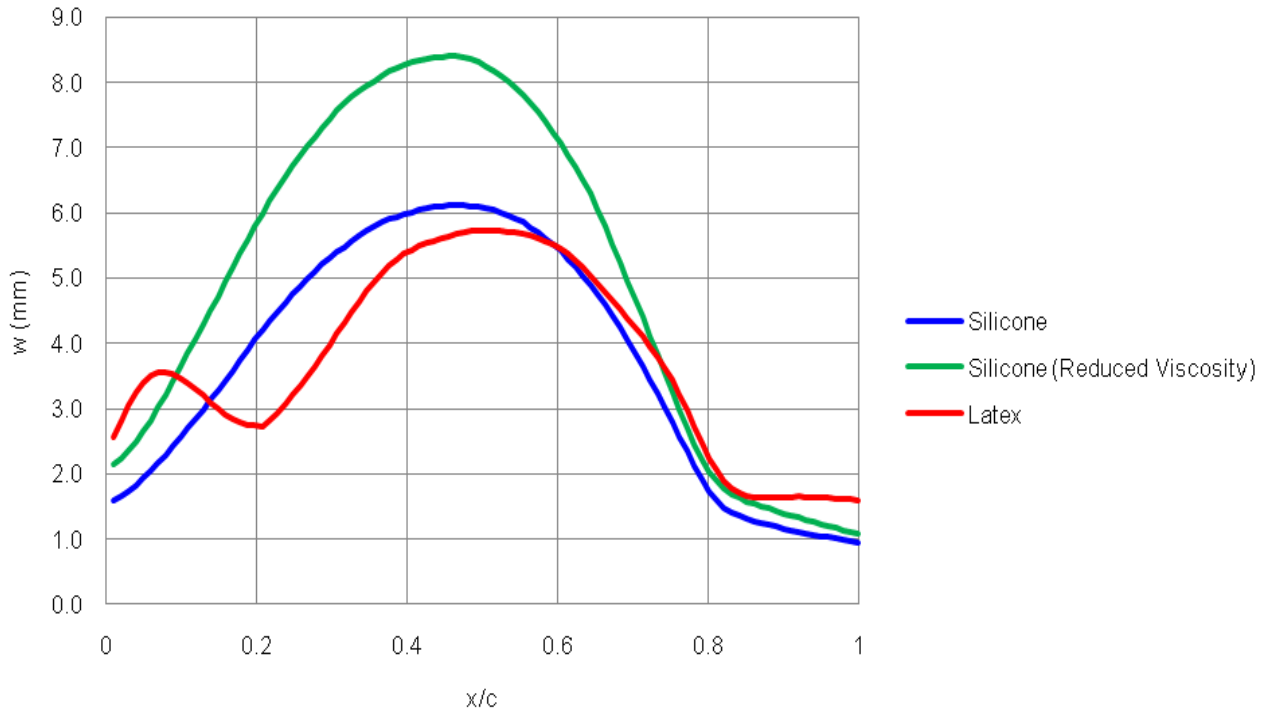


Figure 5-6. Out-of-plane displacements along $2y/b = 0.58$ of various PR membranes, $\alpha = 12^\circ$.

The silicone thinning agent does reduce material strength, which could cause the increased inflation instead of a reduced membrane pre-tension. A weaker membrane would be expected to inflate more under the same loads, and the distinction could not be clarified through these experiments. Future work is recommended to determine the effect of viscosity-reducing agents on material strength. A thermal test, as well as a pressure test, is recommended to determine if pre-tension can be controlled as a function of curing temperature, or vacuum pressure, or both.

Table 5-2. Maximum membrane displacements, PR wing

Membrane	w [mm]	Location (x/c)
Latex	5.74	0.47
Silicone	6.12	0.50
Silicone <small>Reduced Viscosity</small>	7.54	0.50

Topology Optimization Design Comparison

Stanford [4] formulates the computational framework for aeroelastic topology optimization of MAVs. Optimization of laminate topologies and locations is a function of flight condition,

grid density, initial guess, and design metric. Figure 5-7 presents baseline (A, B, D) and topology optimized (C, E) wing designs. Wing C is a lift-augmenting design optimized for maximum lift. Wing E is a lift-alleviating design optimized for minimum lift slope. The top row in Figure 5-7 represents deformations predicted by Stanford [4]. The bottom row depicts experimental out-of-plane deformation results of the same wing designs, fabricated with silicone membranes. Detailed experimental contours are listed in Appendix A. Appendix B lists numerical models gathered by Stanford [4].

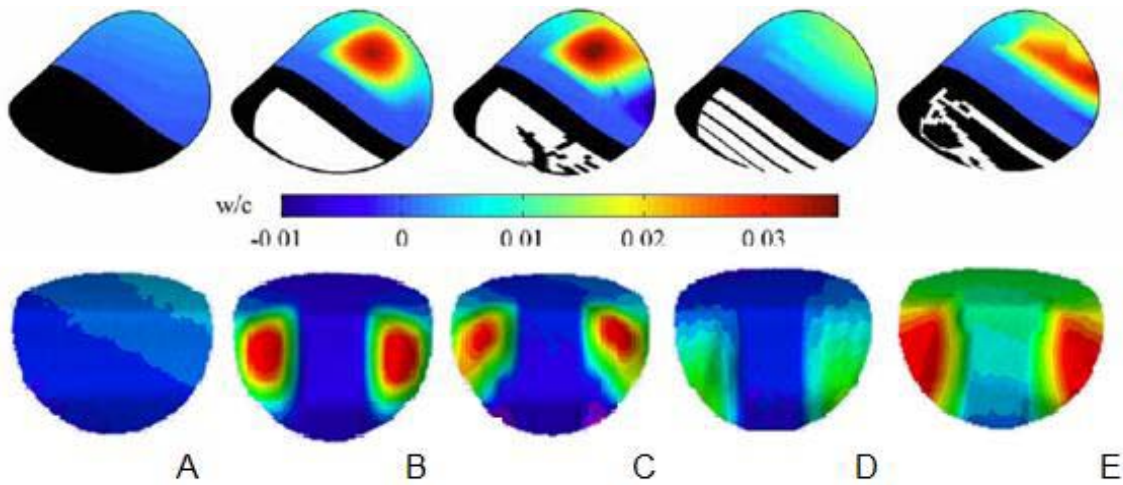


Figure 5-7. Numerical (top) and experimental (bottom) out-of-plane displacements for baseline and topology optimized designs, $\alpha = 12^\circ$.

Figures 5-8 thru 5-13 illustrate comparisons between experimental results and numerical models generated by Stanford [4]. Comparisons are made between baseline and topology optimized designs for different cases. Figures show out-of-plane displacements contours in meters, with experimental results on the left half and its corresponding numerical model on the right half. Since membrane pre-tension parameters were not equal for the two models, a difference in maximum displacement values is expected (Table 5-3). It is more significant to note the shape similarities displayed in the following comparisons.

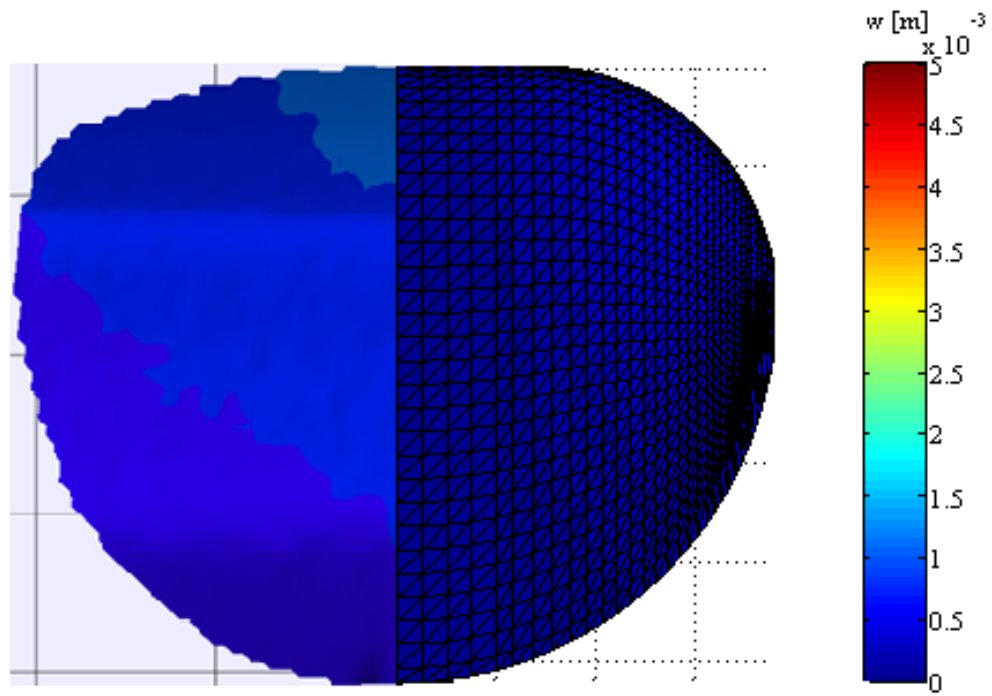


Figure 5-8. Experimental (left) and numerical (right) out-of-plane displacements, rigid wing, $\alpha = 12^\circ$.

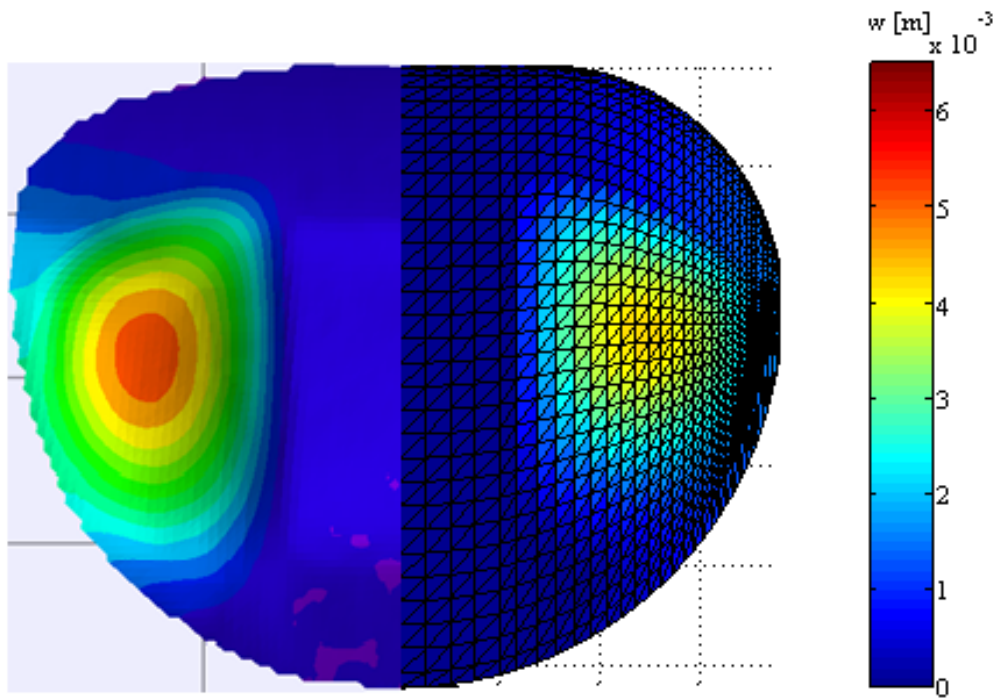


Figure 5-9. Experimental (left) and numerical (right) out-of-plane displacements, PR wing, $\alpha = 12^\circ$.

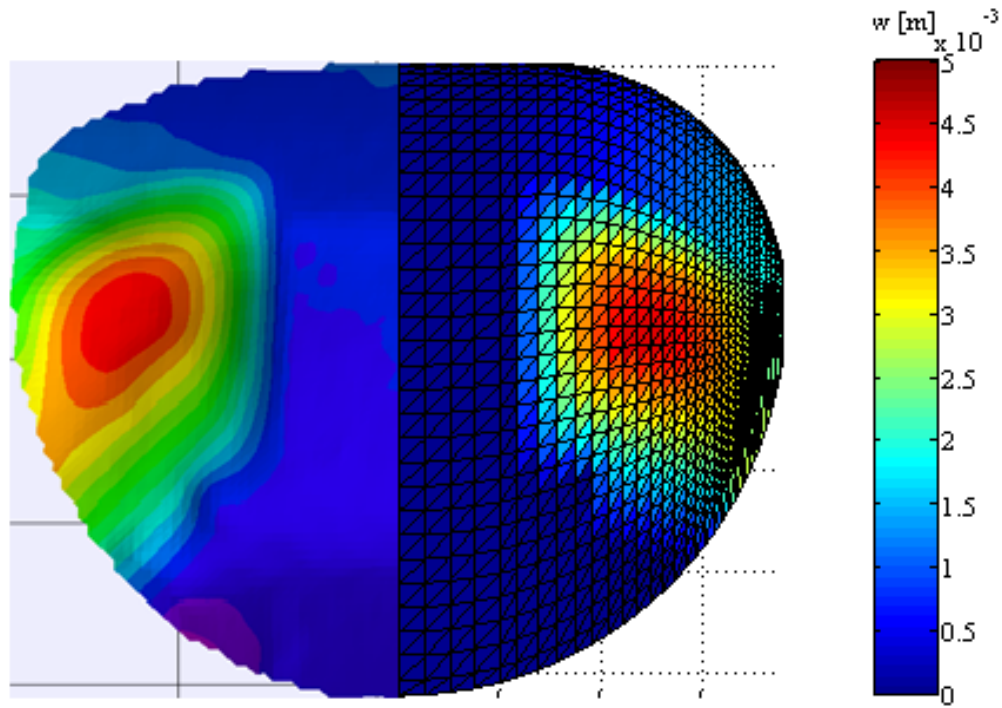


Figure 5-10. Experimental (left) and numerical (right) out-of-plane displacements, topology optimized wing for maximum lift ($TOP_{\max \text{ lift}}$), $\alpha = 12^\circ$.

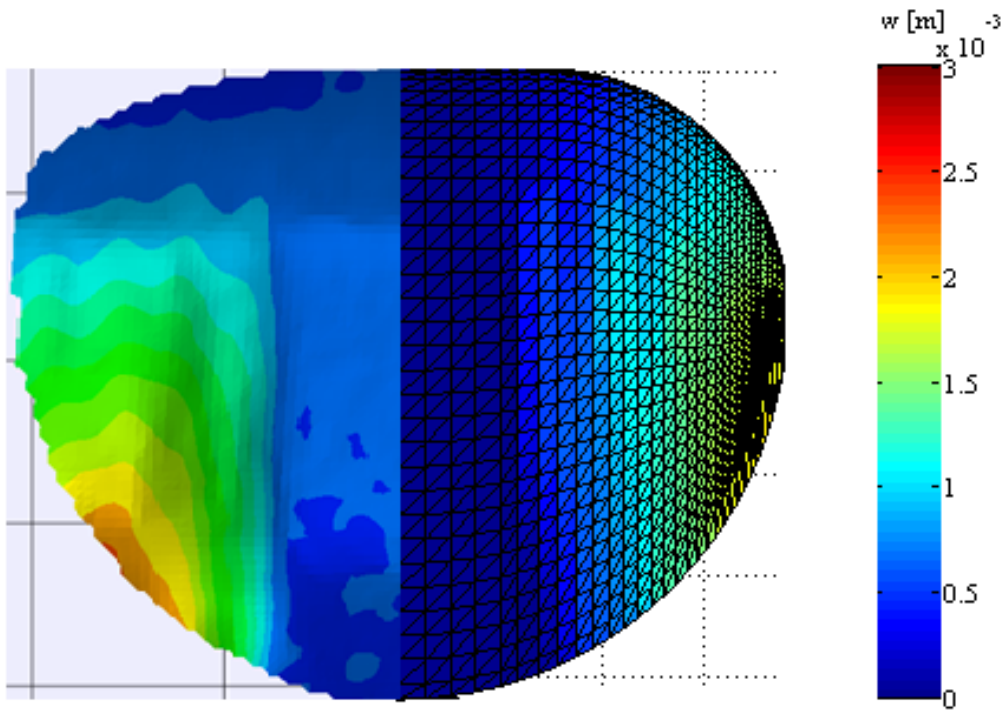


Figure 5-11. Experimental (left) and numerical (right) out-of-plane displacements, BR wing, $\alpha = 12^\circ$.

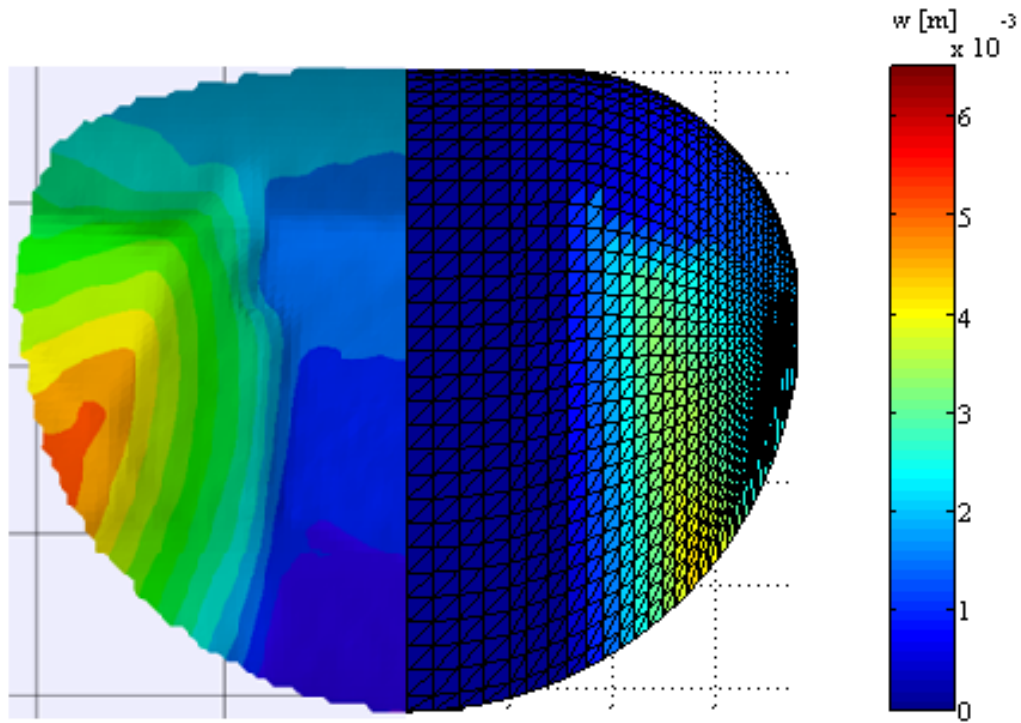


Figure 5-12. Experimental (left) and numerical (right) out-of-plane displacements, topology optimized wing for minimum lift slope ($TOP_{\min \text{ lift slope}}$), $\alpha = 12^\circ$.

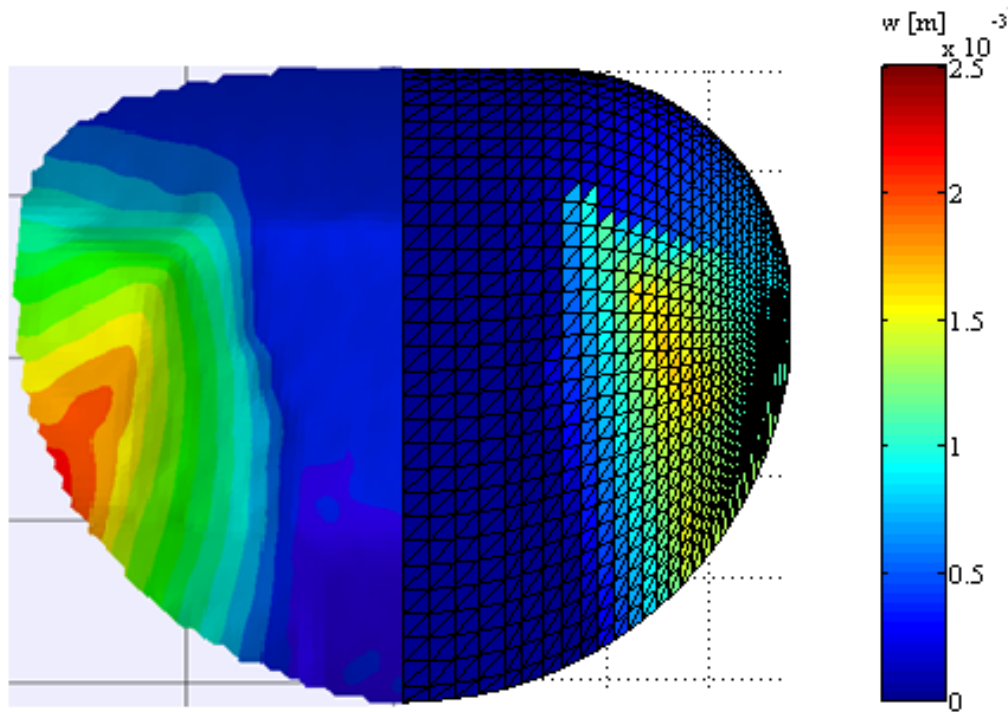


Figure 5-13. Experimental (left) and numerical (right) out-of-plane displacements, $\delta = 1.0$ optimization wing for minimum lift slope ($TOP_{\delta=1}$), $\alpha = 12^\circ$.



Figure 5-14. Baseline and TOP design shapes compared in Figures 5-8 through 5-13, respectively from left to right.

Table 5-3 shows differences in maximum out-of-plane displacements between the numerical model and experimental results. Displacement differences can be attributed to membrane pre-tension inequalities between the two models. In other words, experimental membrane pre-tensions and numerical solver input values were not equal, therefore causing inaccuracies in displacement measurements. A true comparison can only be made if both models have equal pre-tension inputs.

Table 5-3. Maximum out-of-plane displacement comparisons, $\alpha = 12^\circ$

Wing	Numerical [mm]	Experimental [mm]	% Diff
Rigid	0.49	1.56	218.37
PR	4.21	6.48	53.92
BR	1.89	2.59	37.04
TOP _{max lift}	4.53	5.17	14.13
TOP _{min lift slope}	4.25	4.79	12.71
TOP _{$\delta=1$}	1.68	1.61	4.17

In Figure 5-15, experimental results (left) are compared with numerical models (right) for baseline and optimal topology designs. Values are normalized by the root chord and measured approximately along the spanwise section $2y/b = 0.58$. Experimental displacements are reasonably consistent with predicted results. The PR wing did, however, outperform the wing optimized for maximum lift. The wing optimized for minimum lift also exceeded predicted results, but was within range compared to the other designs.

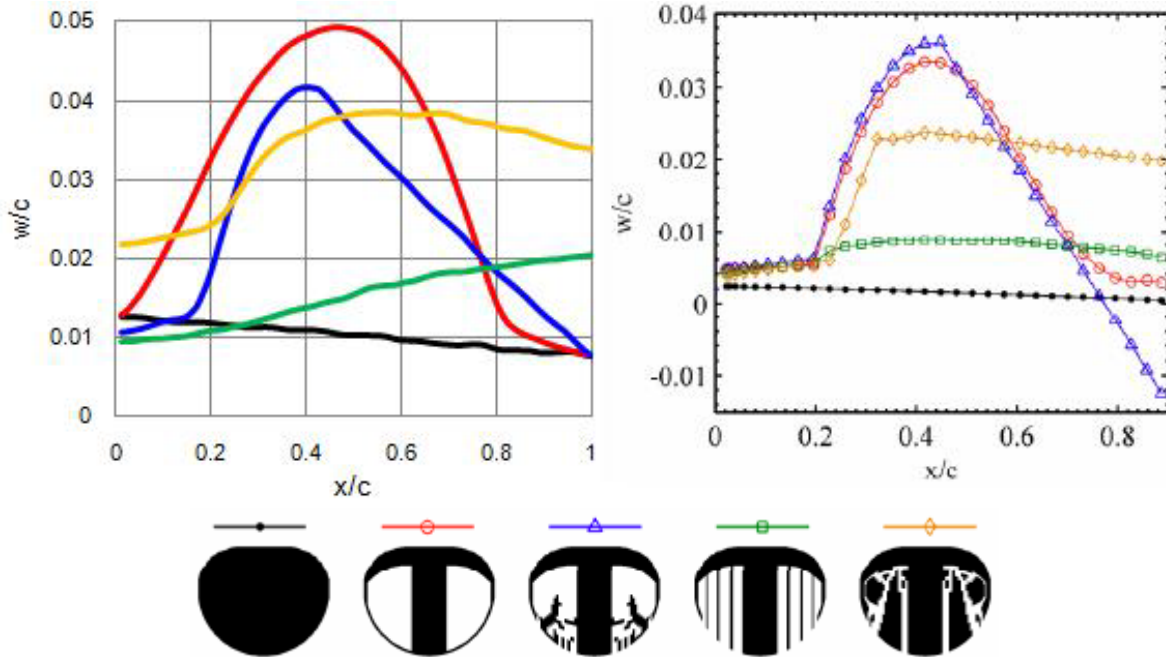


Figure 5-15. Experimental (left) and numerical (right) out-of-plane displacements along $2y/b = 0.58$, baseline and topology designs, $\alpha = 12^\circ$.

Aerodynamic Results

All wind tunnel tests were conducted at $\alpha = 12^\circ$ and $v_\infty = 13$ m/s. Experimental aerodynamic data was collected for two comparative studies. First, the performance of latex membrane and silicone membrane designs was measured using PR and BR wings as baselines. Select aerodynamic coefficients for the PR wing are given in Figure 5-16. BR results are shown in Figure 5-17. The silicone membrane PR wing displayed a shallower lift slope and steeper pitching moment slope. It also had less drag at smaller angles of attack (less than 10°), but higher drag as α increased past 15° . Stall occurred at $\alpha = 22^\circ$ for the silicone membrane PR wing while the latex membrane PR wing stalled at $\alpha = 25^\circ$. Lift data for the BR wing was fairly similar. However, the silicone design outperformed the latex design according to drag and pitching moment.

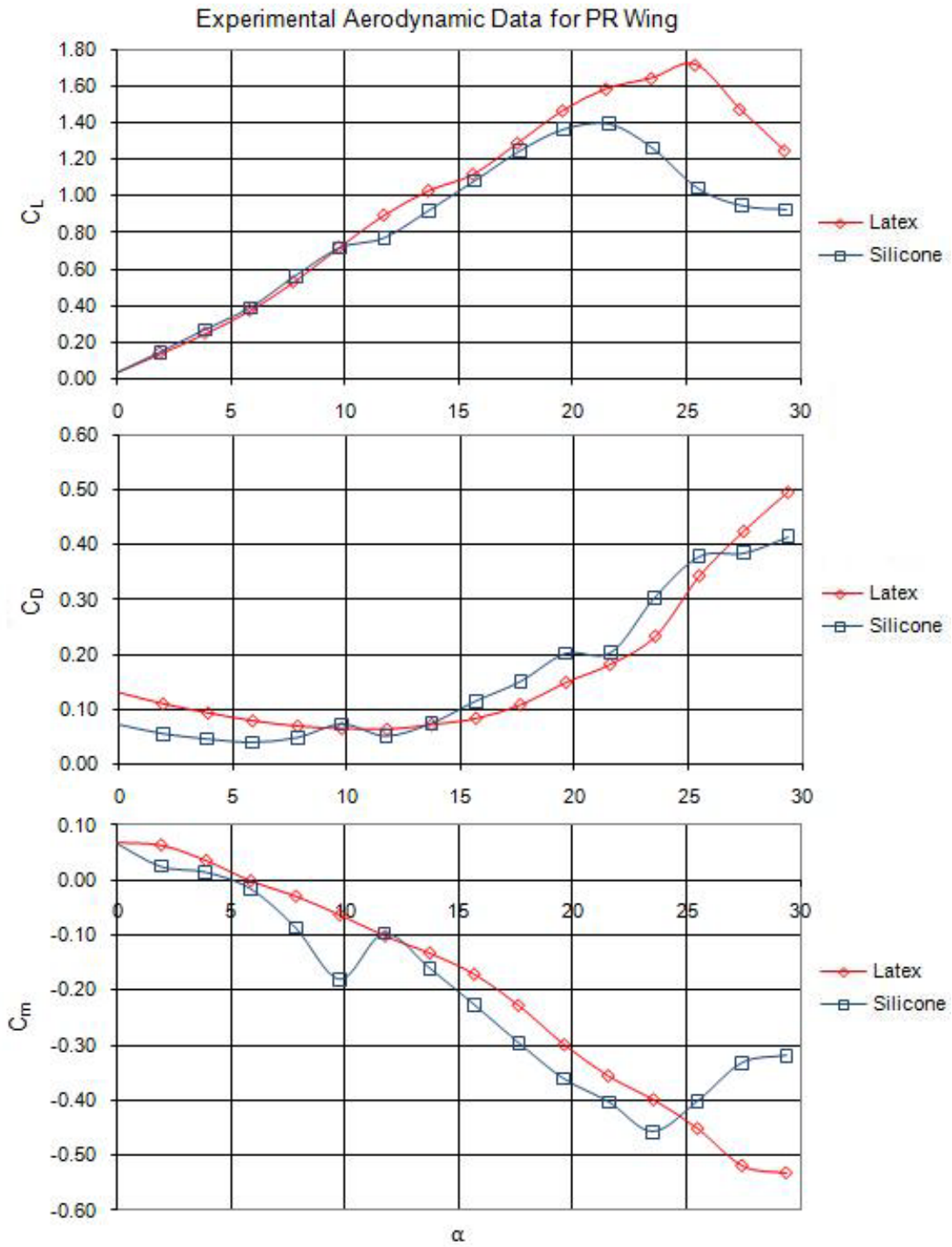


Figure 5-16. Experimental aerodynamic comparison, latex and silicone membrane PR wing, $v_\infty = 13 \text{ m/s}$, $\alpha = 0\text{-}30^\circ$.

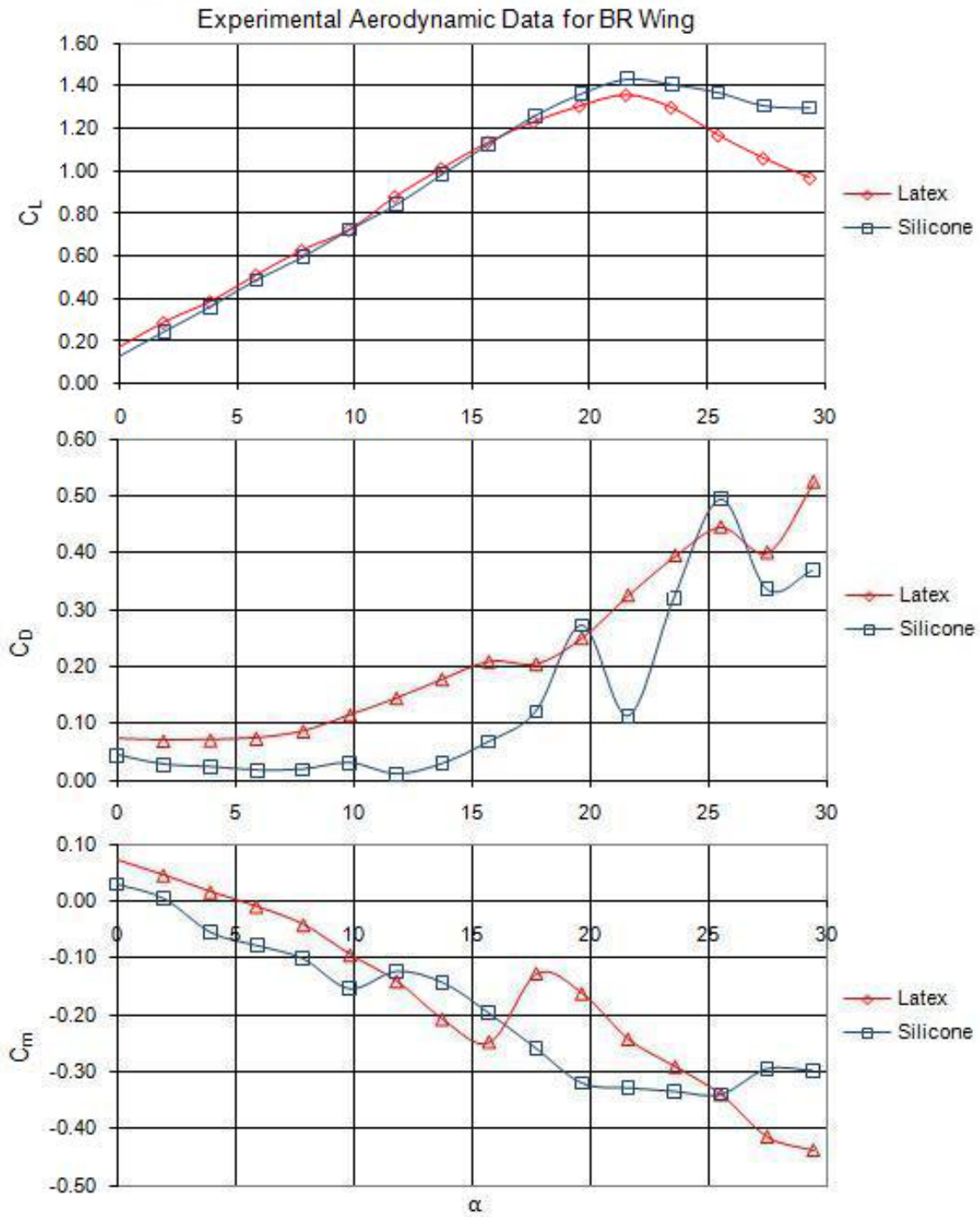


Figure 5-17. Experimental aerodynamic comparison, latex and silicone membrane BR wing, $v_\infty = 13 \text{ m/s}$, $\alpha = 0\text{-}30^\circ$.

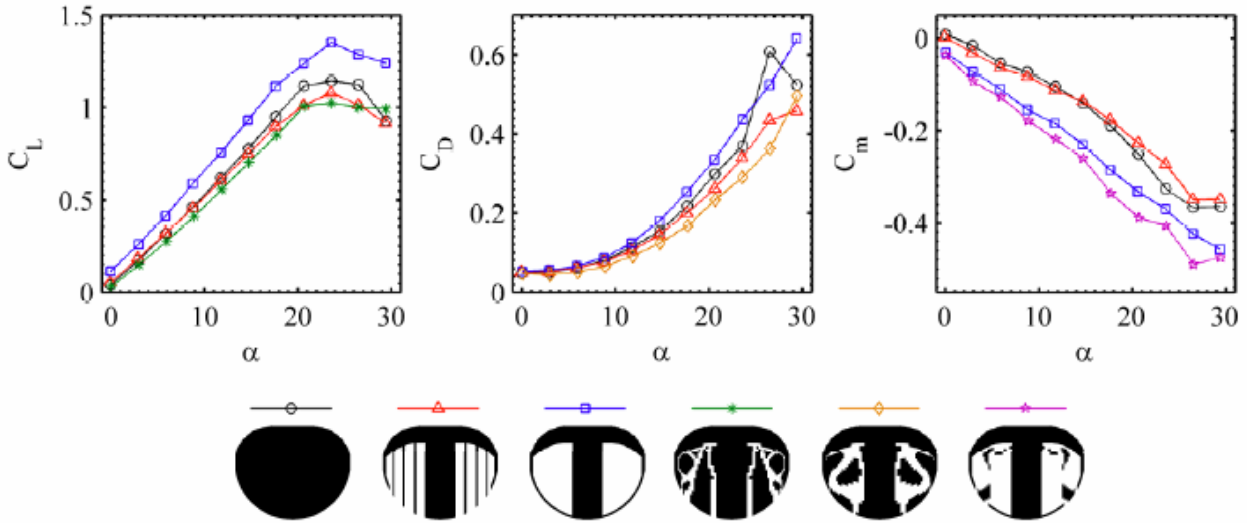


Figure 5-18. Experimental aerodynamic data for low-tensioned, latex membrane baseline and topology optimized designs by Stanford [4], $v_\infty = 13$ m/s, $\alpha = 0-30^\circ$.

Figure 5-18 shows experimental data taken by Stanford [4] for baseline and topology optimized designs for C_L , C_D , and C_m . These wings were constructed with low-tension and latex membranes. Experimental results for corresponding designs are shown in Figure 5-19. All wings were manufactured with silicone membranes with comparable pre-tension in both membranes. The $TOP_{\min C_m}$ design was the most consistent, as it clearly displayed the steepest pitching moment. The $TOP_{\min C_L}$ design exhibited its optimization metric at higher angles of attack ($\alpha > 15^\circ$) while the $TOP_{\min C_D}$ design showed lower drag at lower angles of attack ($\alpha < 20^\circ$). Overall, experimental results were reasonably consistent with their expected behaviors.

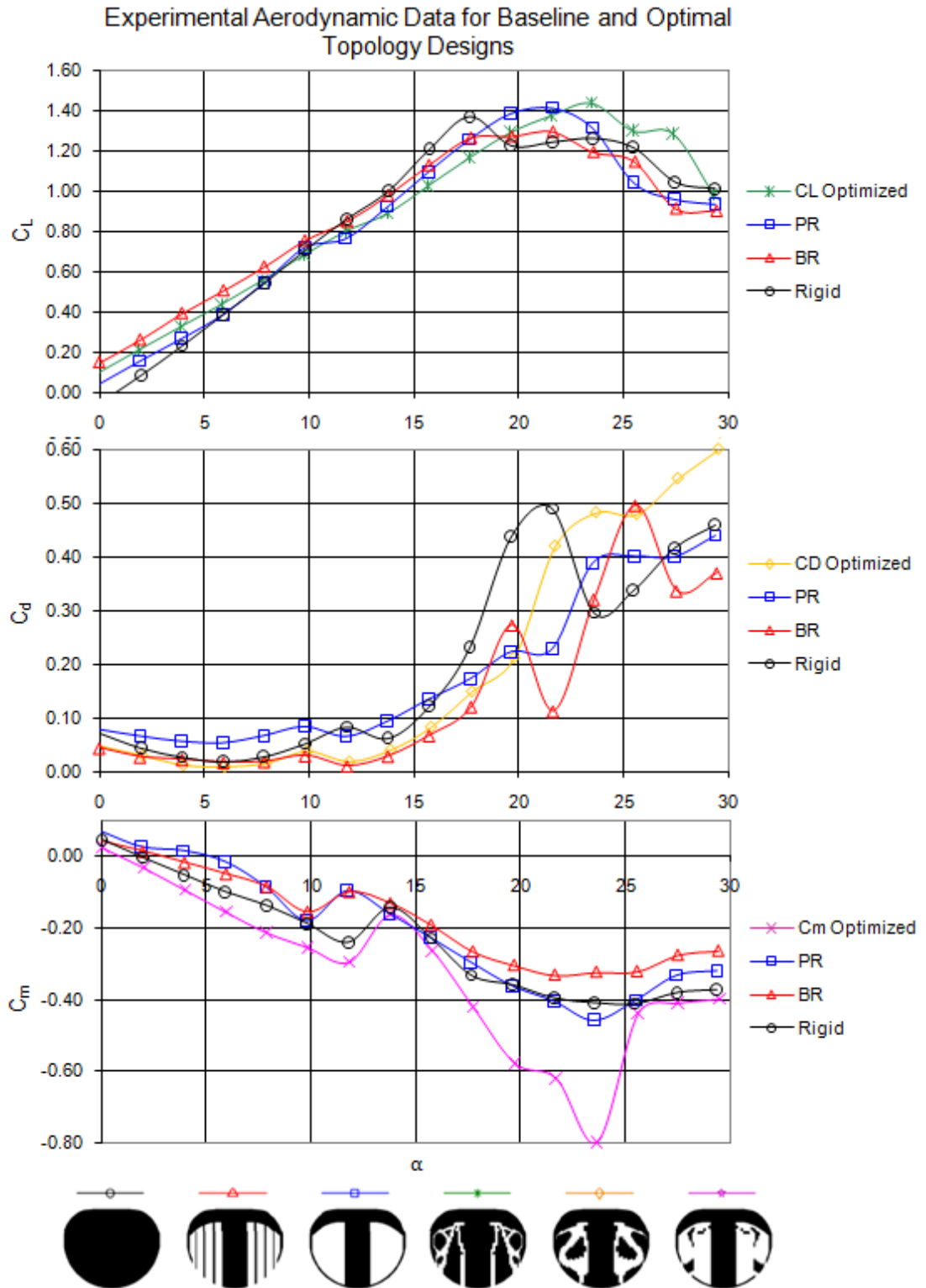


Figure 5-19. Experimental aerodynamic data for uniform-tensioned, silicone membrane baseline and topology optimized designs (from Figure 5-17), $v_\infty = 13$ m/s, $\alpha = 0$ -30°.

CHAPTER 6 RELATED CONCEPTS

Recently, there is heightened interest in developing bio-inspired wings. Much effort has been dedicated to the study of natural flyers in hopes of mimicking beneficial flight characteristics. Silicone membrane manufacturing techniques developed in this work may be helpful in creating designs along the bio-inspiration front, including bat wing designs as expressed in Chapter 2. Composite skeletons could be co-cured with silicone membrane designs to develop very robust and realistic MAVs.

Integrating control surfaces into these membranes is another concept which could further evolve future MAV designs. Figure 6-1 shows the fabrication of such a concept. A modified 24-inch BR MAV wing is integrated with piezoelectric actuators on the wingtips. Pigmented silicone rubber serves as the fusing membrane. Wingtip deflections were observed and comparable with a 24-inch all-carbon fiber wing, also fused with wingtip actuators.

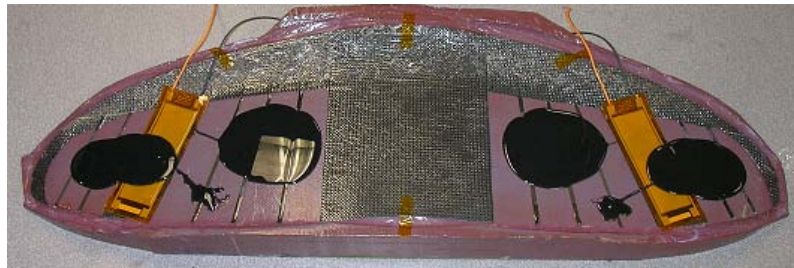


Figure 6-1. Fabrication of 24-inch BR piezoelectric concept wing membrane with pigmented liquid silicone compound.



Figure 6-2. 24-inch BR piezoelectric concept wing.

CHAPTER 7 CONCLUSION

Conclusion

Flexible wing MAVs have two design issues that could be improved and should be addressed. First, current materials used for flexible wing membranes lack durability, robustness, and shelf life. Second, current manufacturing procedures are unable to create flexible wing membranes displaying consistent uniform pre-tension. Silicone rubber was identified as an ideal membrane material because of its superior thermal properties, highly inert nature, and resistance to environmental factors such as ozone, radiation, heat, and moisture. A manufacturing process was developed to cure liquid silicone rubber onto composite laminate wing structures, successfully fabricating membranes of uniform pre-tension.

Experimental VIC data was gathered to validate this claim, using the PR design as the baseline. Furthermore, membrane inflation controllability was observed by adjusting the viscosity of the silicone solution (also validated with VIC). Aeroelastic comparisons with latex membrane platforms revealed the superiority of silicone membranes. Results indicated symmetric out-of-plane displacements across both silicone membranes, unlike those with latex membranes. Numerical models of selected topology optimized designs were compared with experimental results, yielding similar displacement contours. There was some variation in maximum membrane displacements, as pre-tensions of the experimental models and numerical solver inputs were unequal.

Future Work

Future work should be carried out to perfect the silicone membrane co-curing manufacturing process of MAVs. Areas of focus should include:

1. Measuring silicone adhesion strength to composite structures over a range of curing temperatures.

2. Developing a relationship between liquid silicone viscosity and cured material strength.
3. Developing a relationship between membrane thickness and strength.
4. Conducting a thermal test to determine if pre-tension can be controlled as a function of silicone curing temperature.
5. Conducting a pressure test to determine if pre-tension can be controlled as a function of vacuum pressure.
6. Creating precision-machined wing molds specifically for silicone membrane applications.
7. Developing bio-inspired wings using composite skeletons fused into silicone membranes.
8. Integrating control surfaces (such as piezoelectric actuators) into silicone membrane wings.
9. Building and flying prototype MAVs.

APPENDIX A
EXPERIMENTAL OUT-OF-PLANE DISPLACEMENT CONTOURS FOR BASELINE AND
TOPOLOGY OPTIMIZED WING DESIGNS

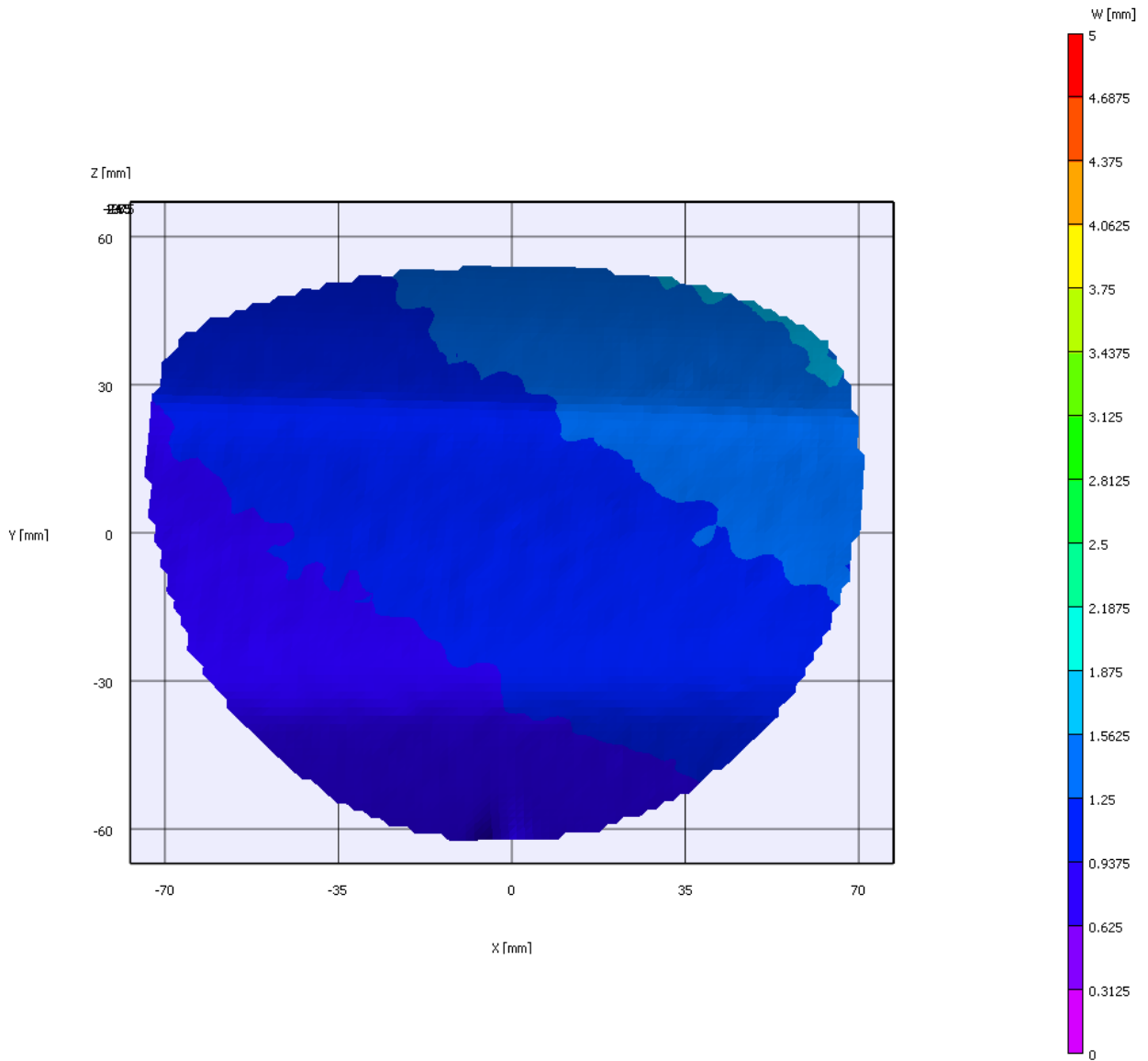


Figure A-1. Experimental out-of-plane displacement contour, rigid wing, $\alpha = 12^\circ$.

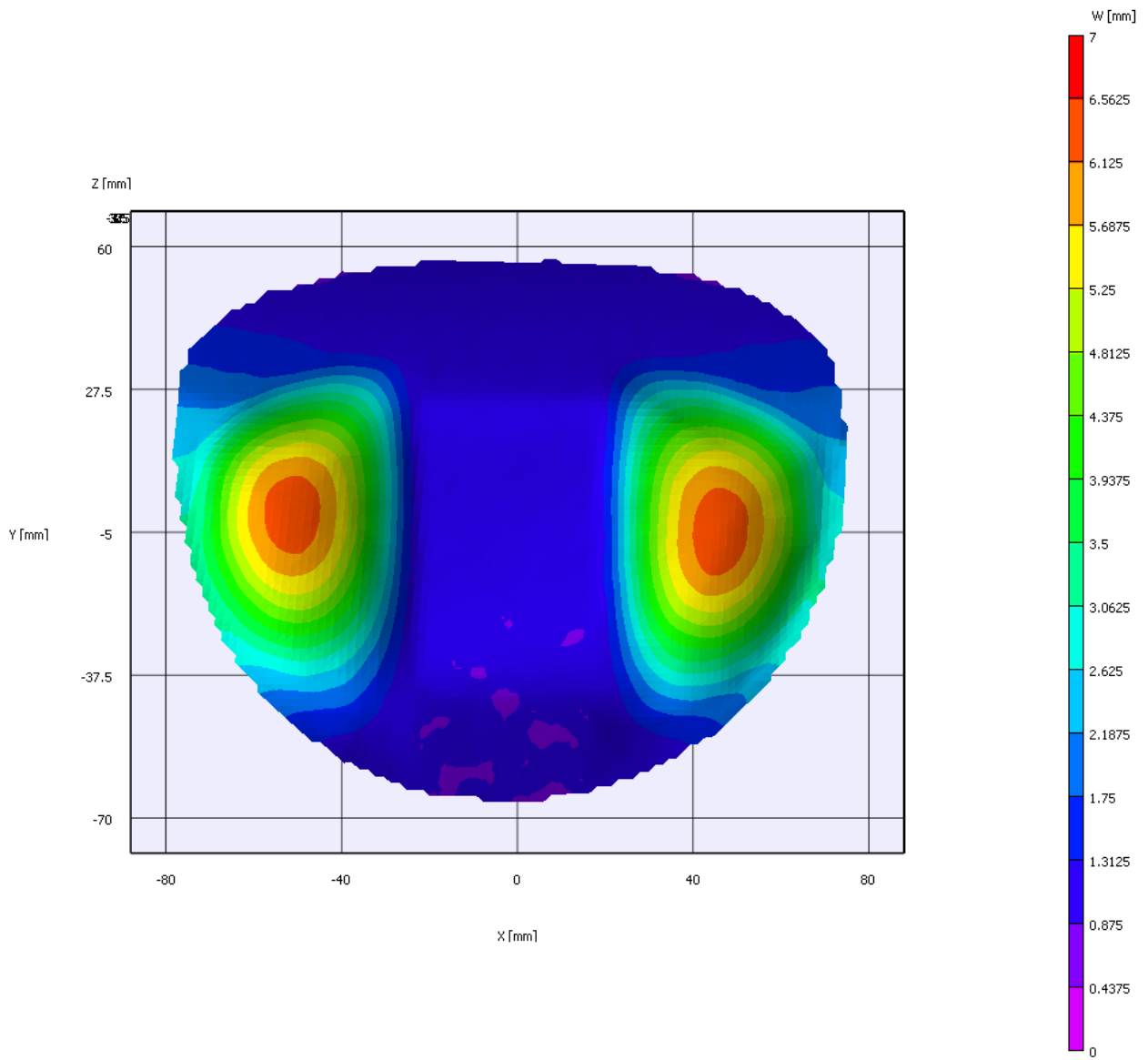


Figure A-2. Experimental out-of-plane displacement contour, silicone membrane PR wing, $\alpha = 12^\circ$.

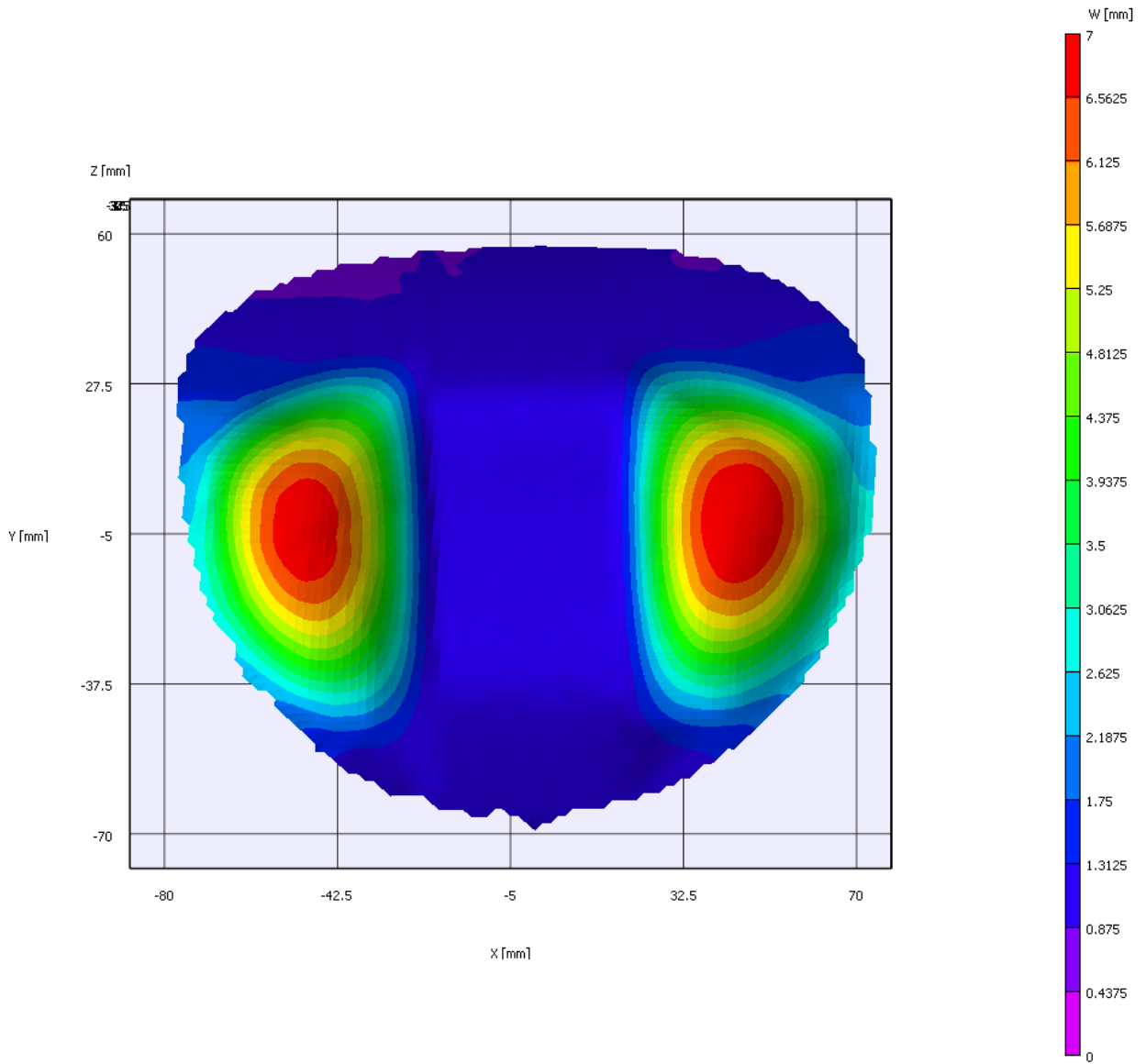


Figure A-3. Experimental out-of-plane displacement contour, viscosity-reduced silicone membrane PR wing, $\alpha = 12^\circ$.

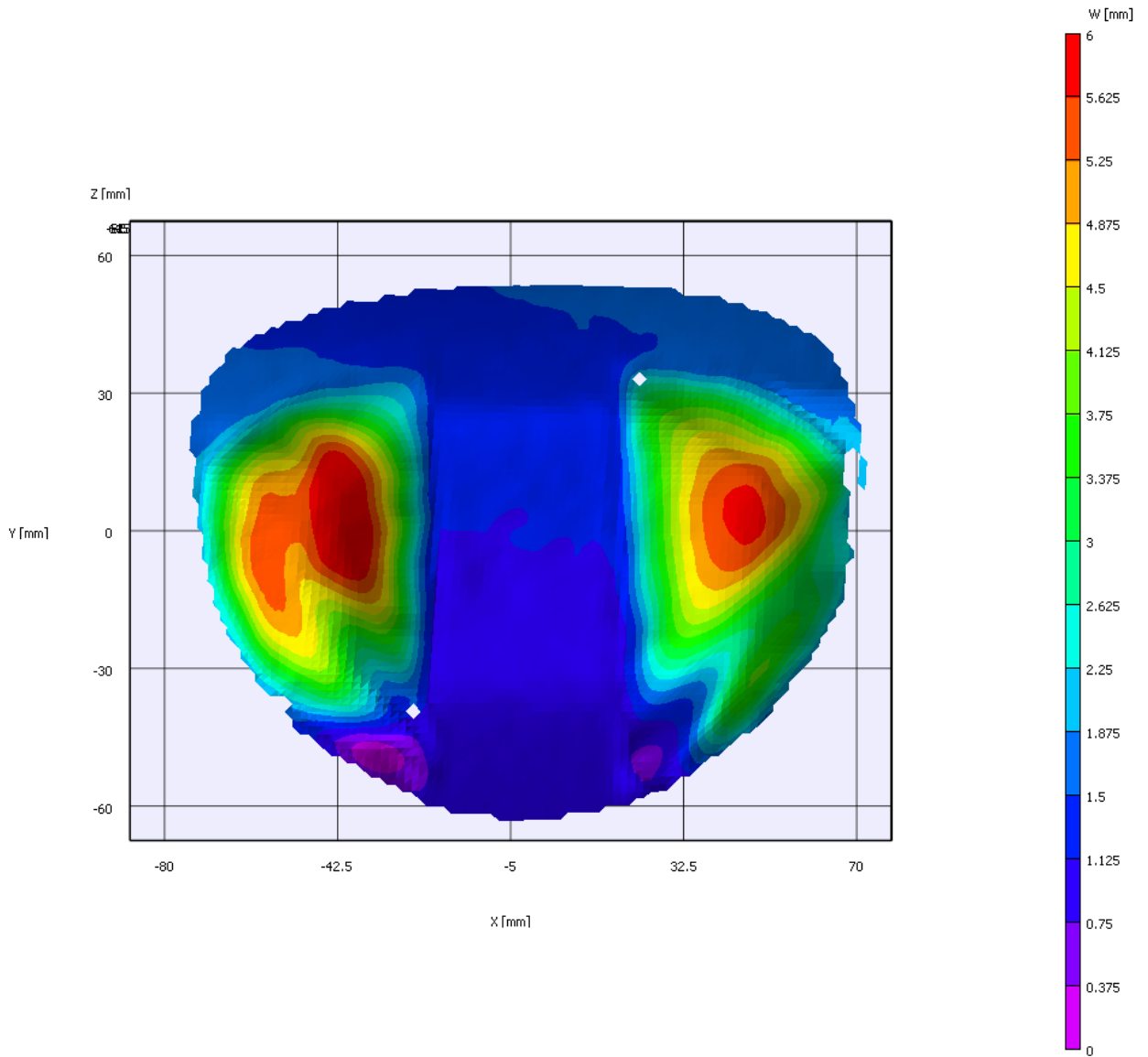


Figure A-4. Experimental out-of-plane displacement contour, latex membrane PR wing, $\alpha = 12^\circ$.

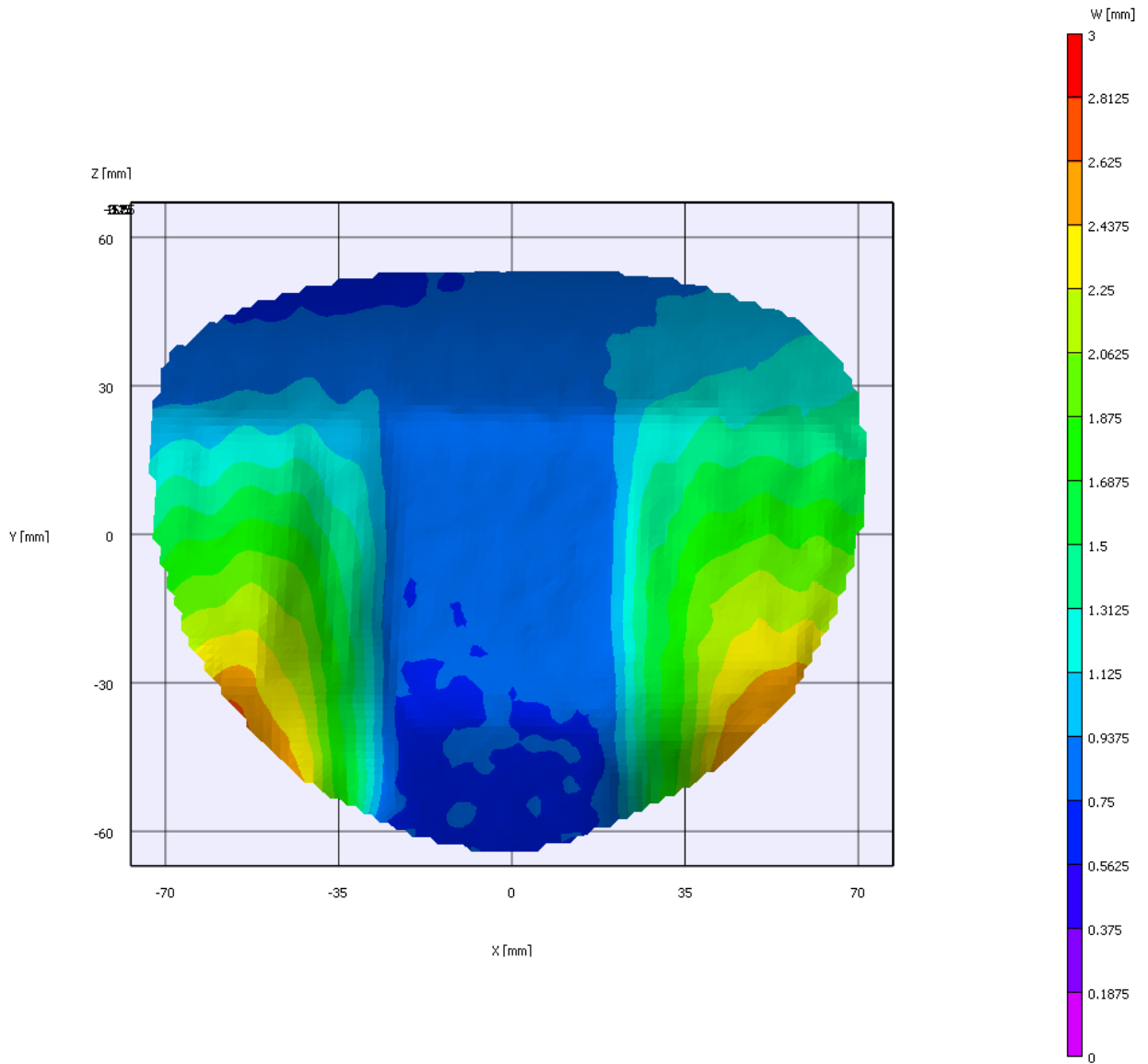


Figure A-5. Experimental out-of-plane displacement contour, silicone membrane BR wing, $\alpha = 12^\circ$.

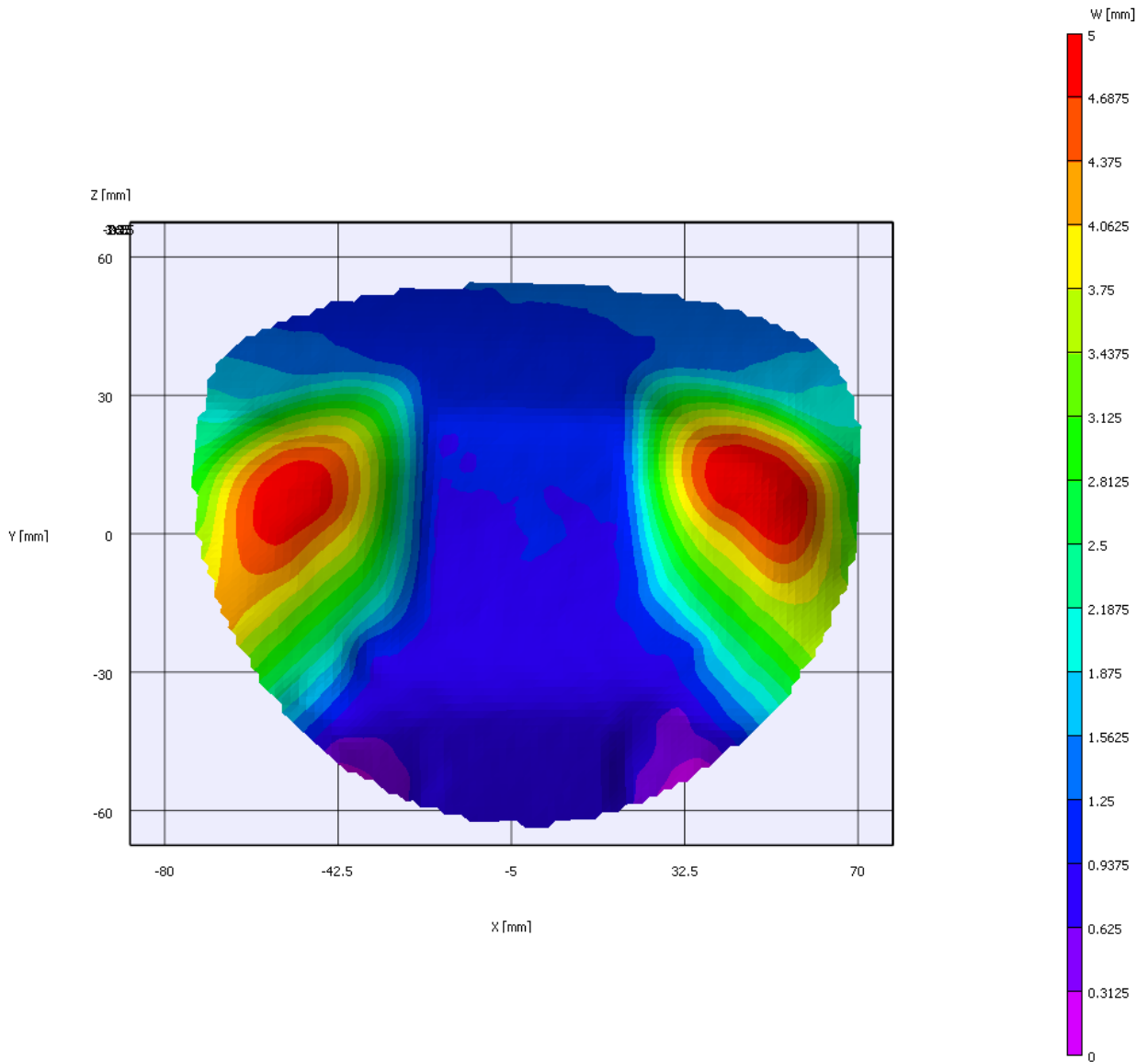


Figure A-6. Experimental out-of-plane displacement contour, silicone membrane TOP wing optimized for maximum lift ($TOP_{\max \text{ lift}}$), $\alpha = 12^\circ$ (refer [4], Figure 7-10).

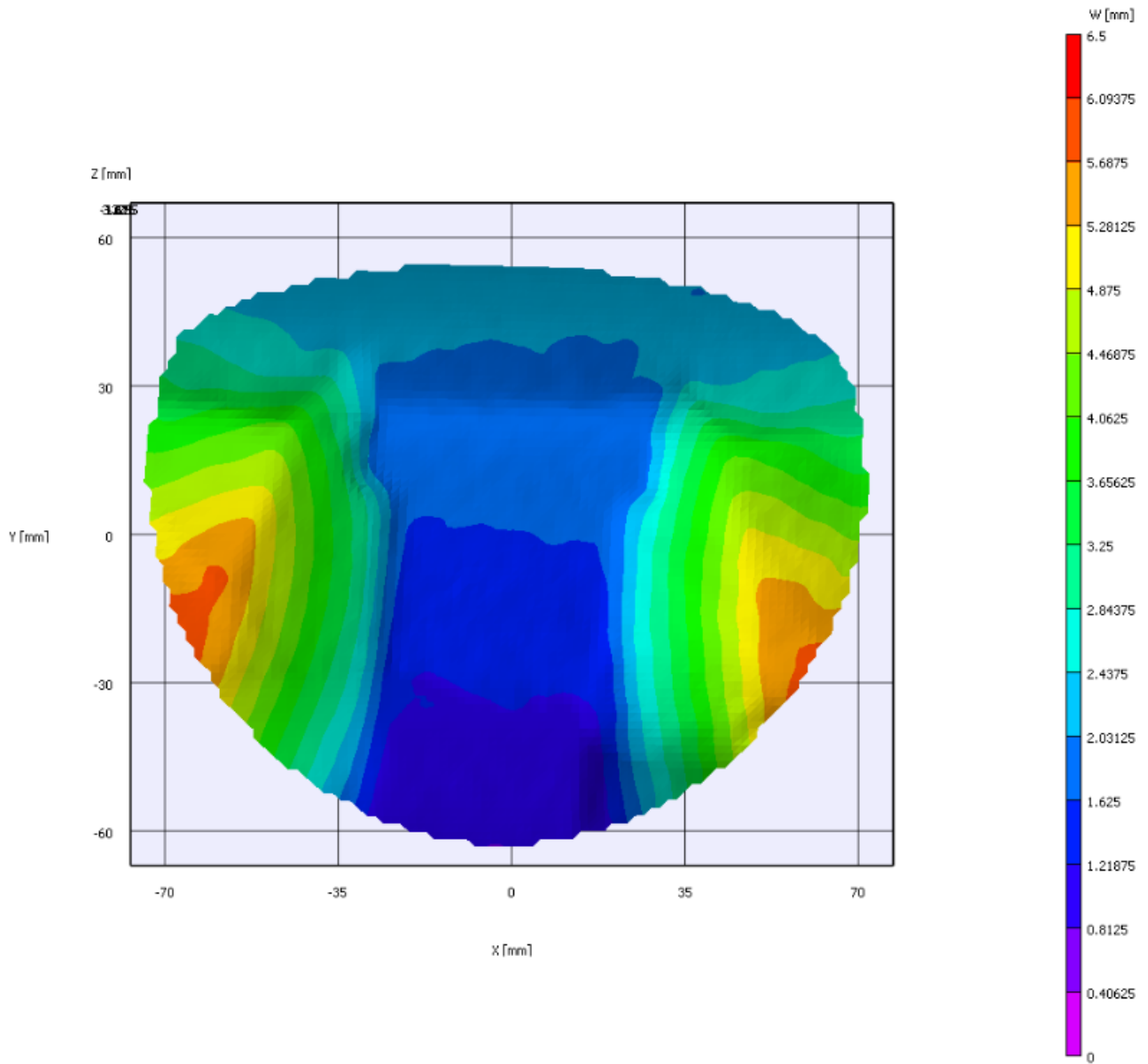


Figure A-7. Experimental out-of-plane displacement contour, silicone membrane TOP wing optimized for minimum lift slope ($TOP_{\min \text{ lift slope}}$), $\alpha = 12^\circ$ (refer [4], Figure 7-10).

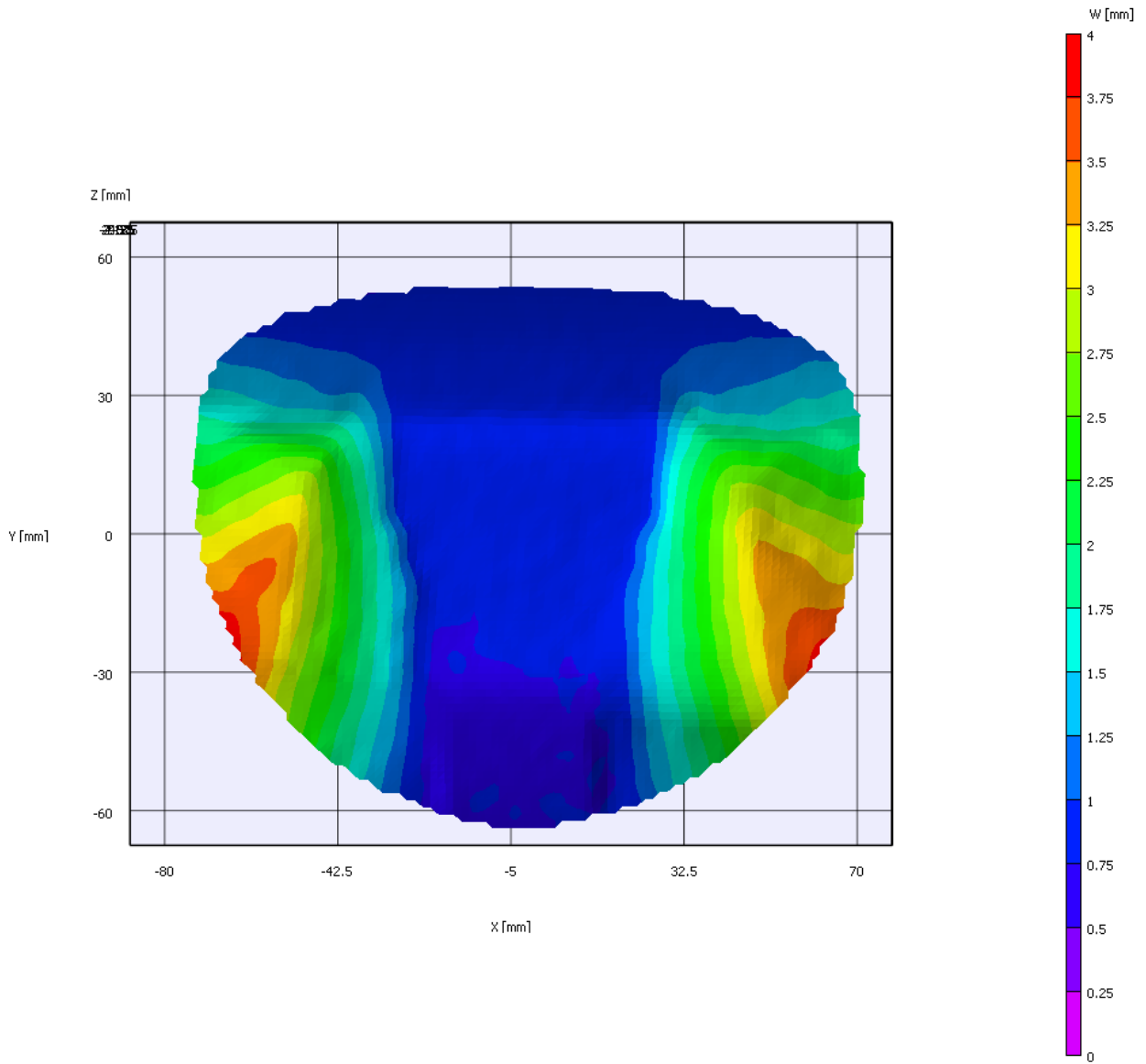


Figure A-8. Experimental out-of-plane displacement contour, silicone membrane TOP wing optimized for minimum C_L ($TOP_{\min CL}$), $\alpha = 12^\circ$ (refer [4], Figure 7-15).

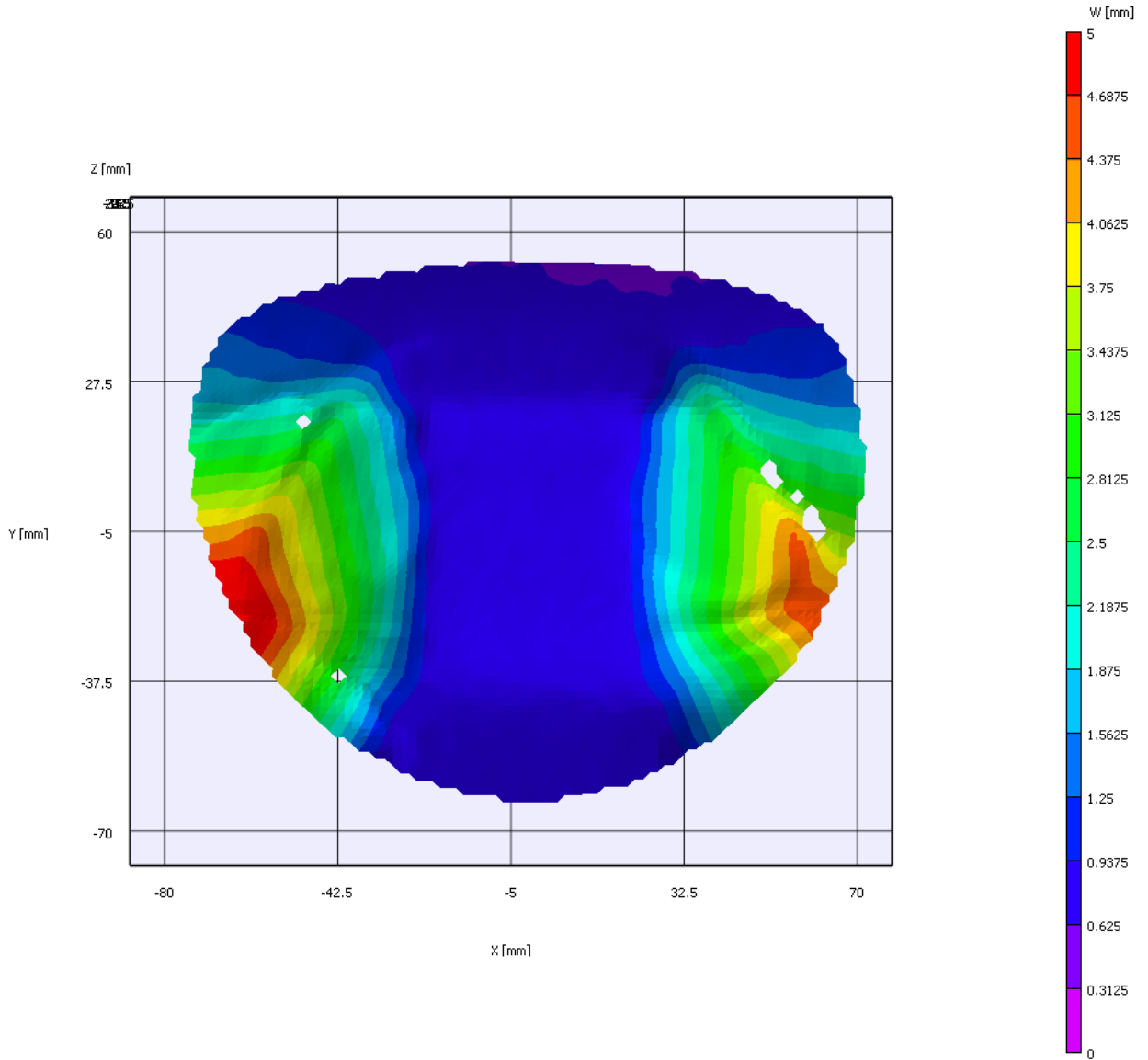


Figure A-9. Experimental out-of-plane displacement contour, silicone membrane TOP wing optimized for minimum C_D ($TOP_{\min C_D}$), $\alpha = 12^\circ$ (refer [4], Figure 7-15).

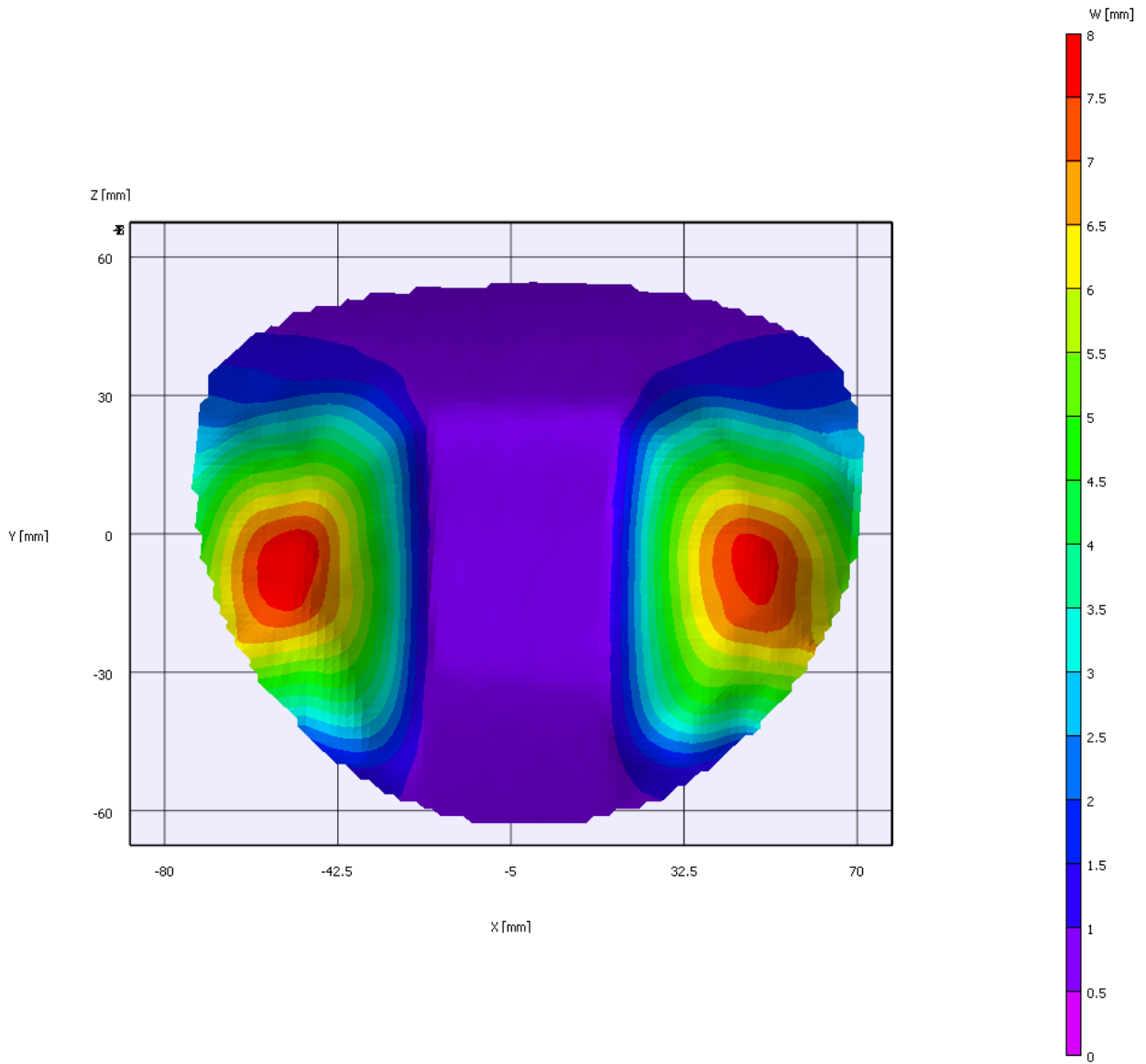


Figure A-10. Experimental out-of-plane displacement contour, silicone membrane TOP wing optimized for minimum C_m ($TOP_{\min C_m}$), $\alpha = 12^\circ$ (refer [4], Figure 7-15).

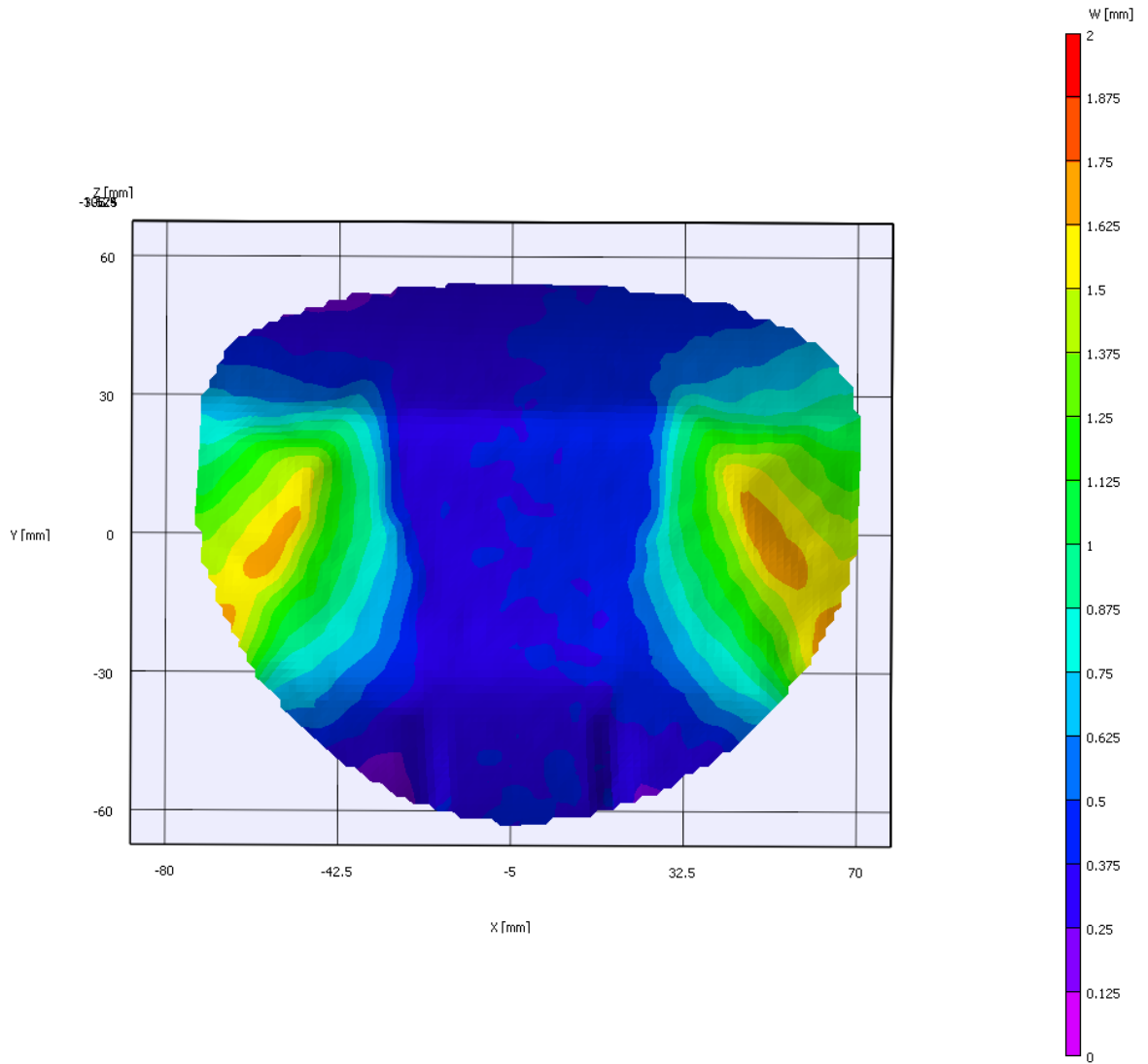


Figure A-11. Experimental out-of-plane displacement contour, silicone membrane TOP wing, single-objective ($\delta = 1.0$) optimized for minimum lift slope ($TOP_{\delta=1}$), $\alpha = 12^\circ$ (refer [4], Figure 7-18).

APPENDIX B
NUMERICAL OUT-OF-PLANE DISPLACEMENT MODELS FOR BASELINE AND
TOPOLOGY OPTIMIZED WING DESIGNS, COURTESY OF STANFORD [4]

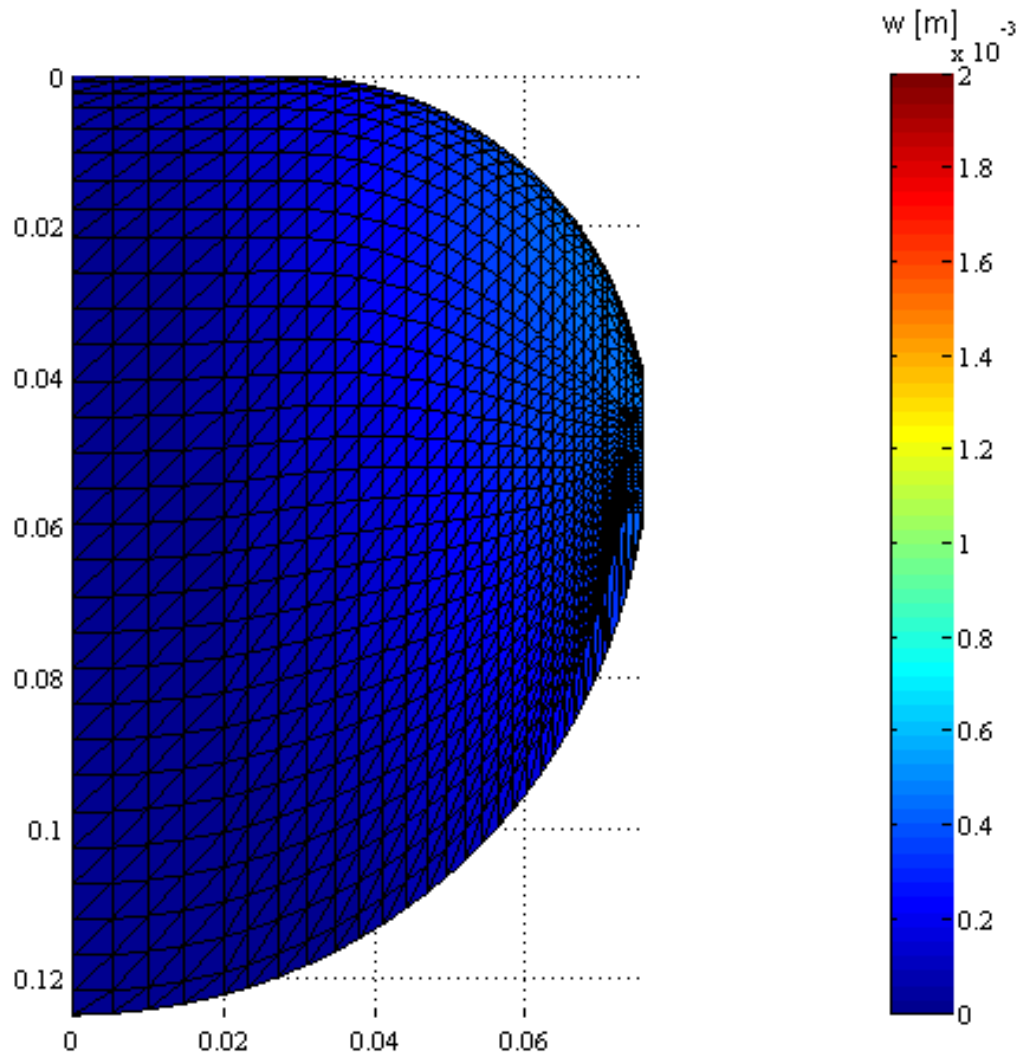


Figure B-1. Numerical out-of-plane displacement model, rigid wing, $\alpha = 12^\circ$.

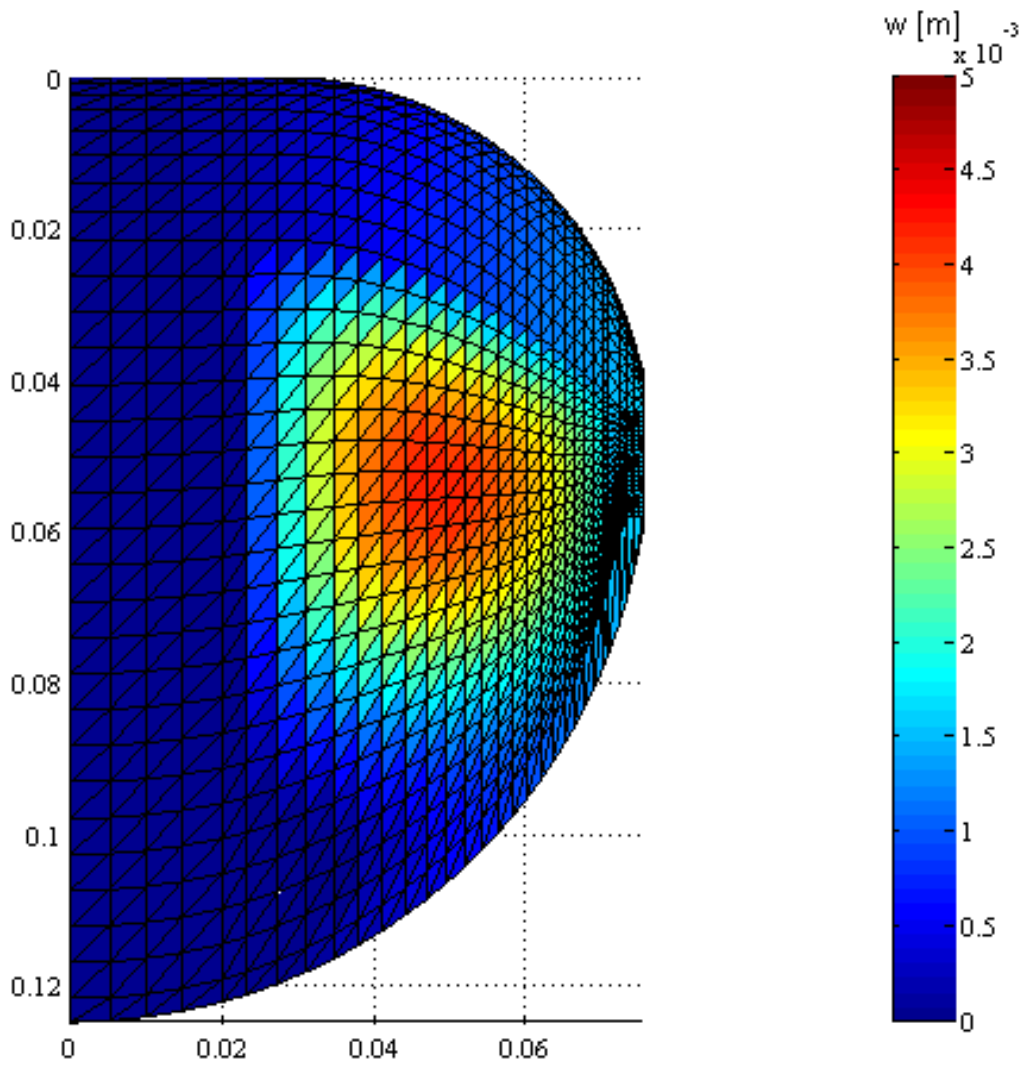


Figure B-2. Numerical out-of-plane displacement model, PR wing, $\alpha = 12^\circ$.

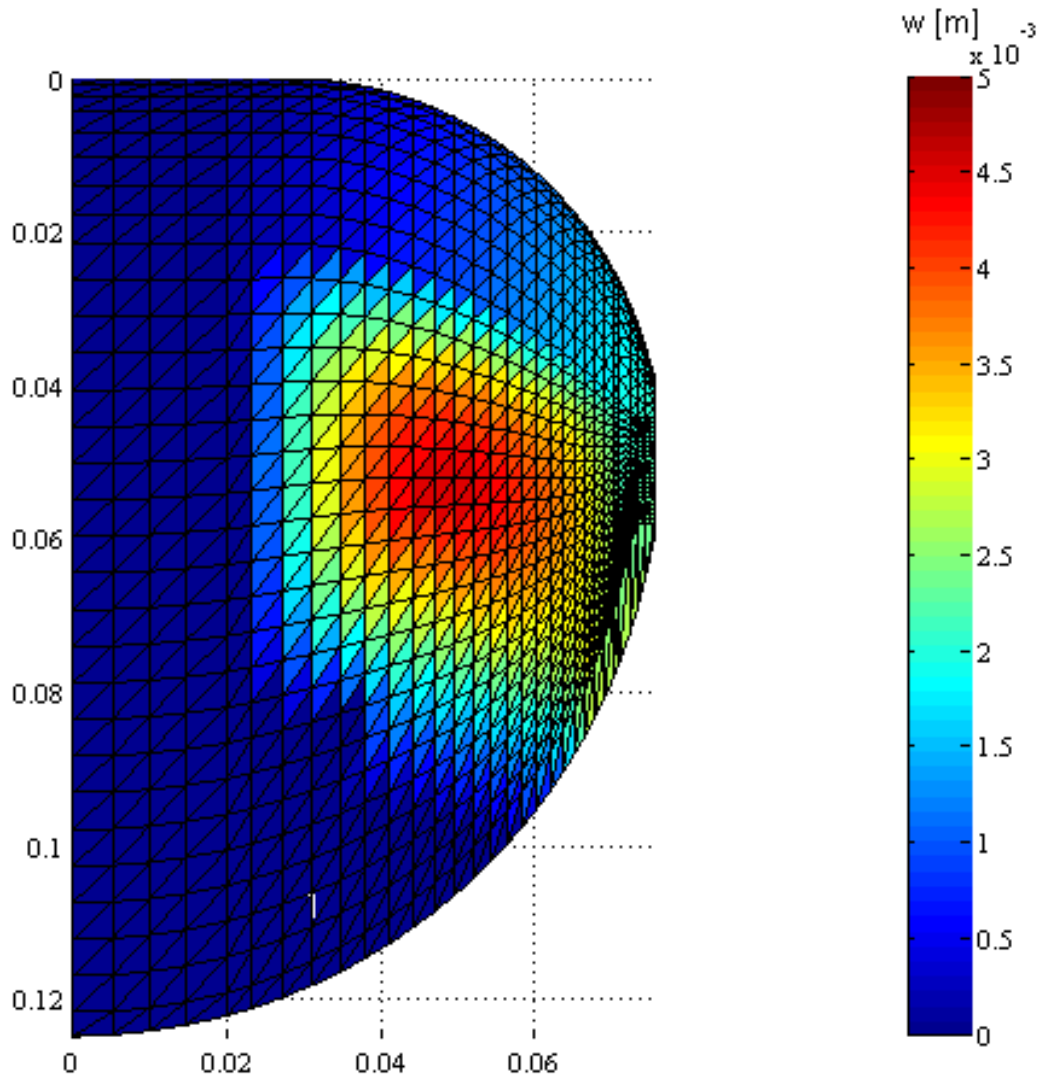


Figure B-3. Numerical out-of-plane displacement model, silicone membrane TOP wing optimized for maximum lift ($TOP_{\max \text{ lift}}$), $\alpha = 12^\circ$ (refer [4], Figure 7-10).

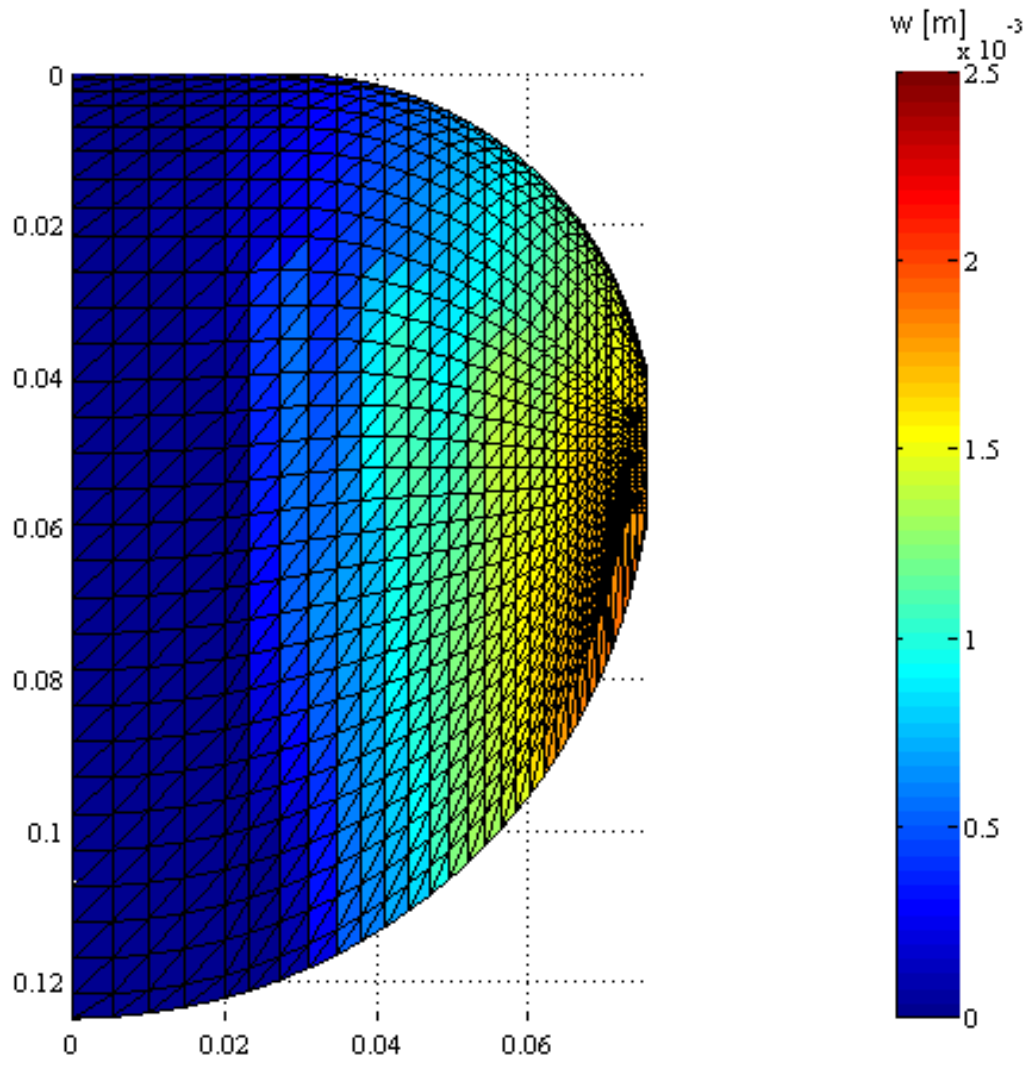


Figure B-4. Numerical out-of-plane displacement model, BR wing, $\alpha = 12^\circ$.

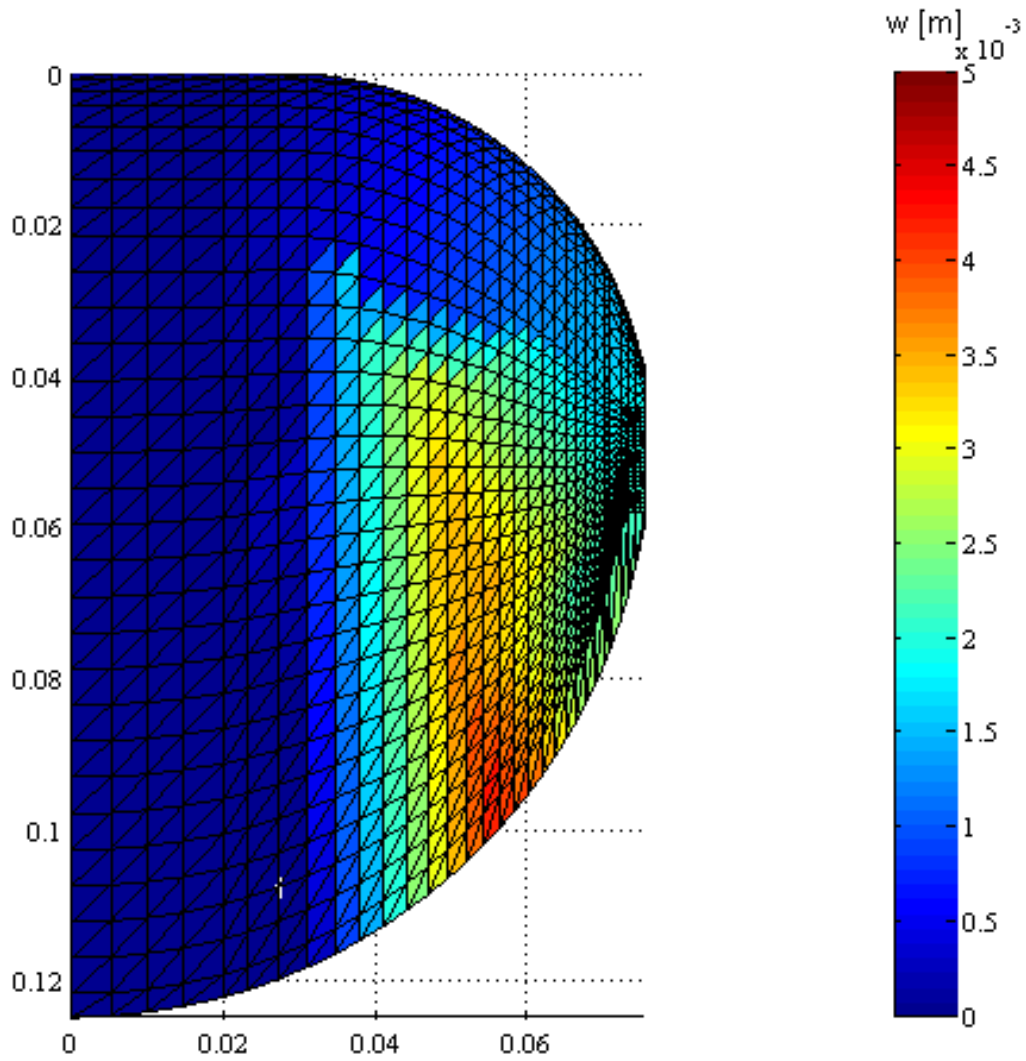


Figure B-5. Numerical out-of-plane displacement model, silicone membrane TOP wing optimized for minimum lift slope ($TOP_{\min \text{ lift slope}}$), $\alpha = 12^\circ$ (refer [4], Figure 7-10).

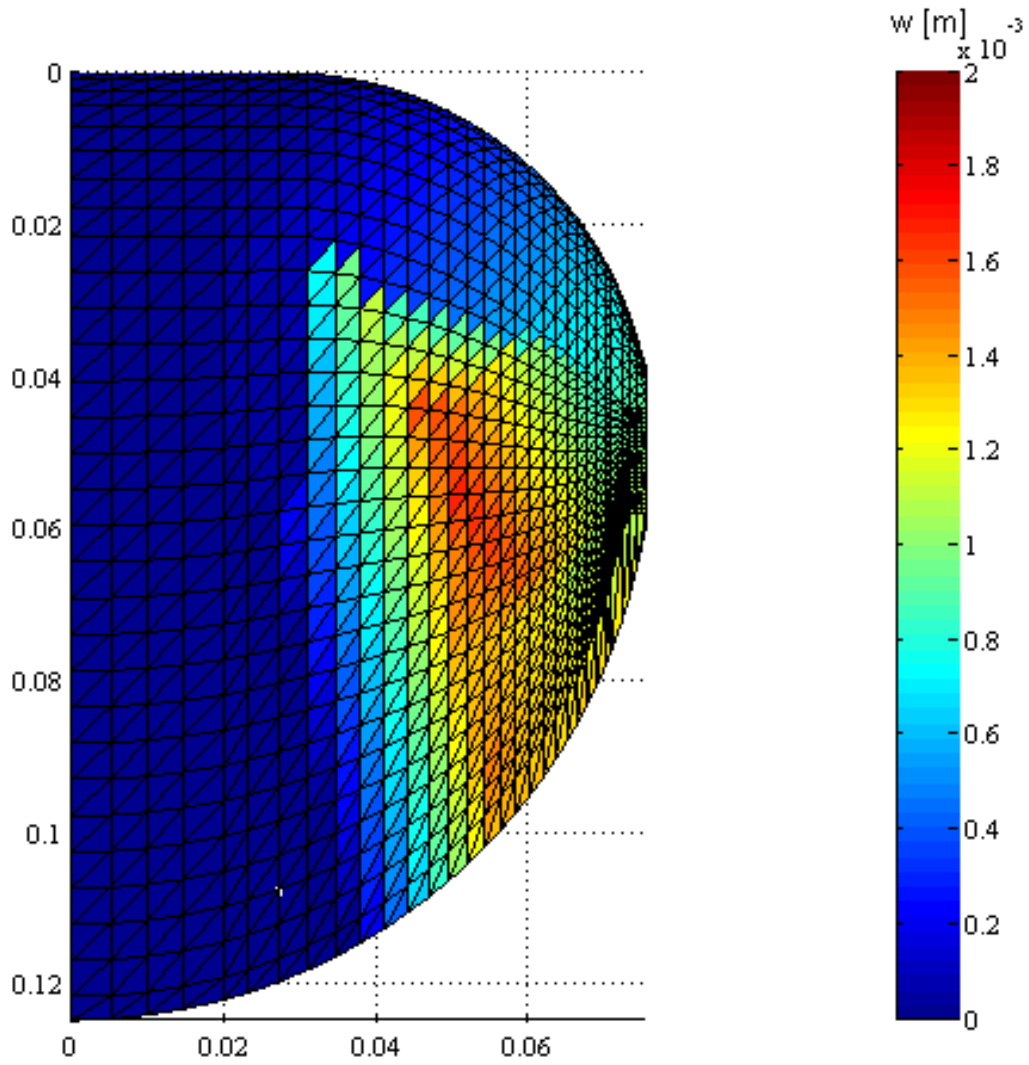


Figure B-6. Numerical out-of-plane displacement model, silicone membrane TOP wing, single-objective ($\delta = 1.0$) optimized for minimum lift slope ($TOP_{\delta=1}$), $\alpha = 12^\circ$ (refer [4], Figure 7-18).

LIST OF REFERENCES

- [1] Stanford, B., Ifju, P., Albertani, R., Shyy, W., “Fixed Membrane Wings for Micro Air Vehicles: Experimental Characterization, Numerical Modeling, and Tailoring,” *Progress in Aerospace Sciences*, Vol.44, No. 4, 2008, pp. 258-294.
- [2] Ifju, P., Jenkins, D., Ettinger, S., Lian, Y., Shyy, W., Waszak, M., “Flexible-Wing-Based Micro Air Vehicles,” 40th AIAA Aerospace Sciences Meeting & Exhibit, Reno, NV, AIAA Paper 2002-0705, 2002.
- [3] Stanford, B., Ifju, P., “Membrane Micro Air Vehicles with Adaptive Aerodynamic Twist: Numerical Modeling,” *Journal of Aerospace Engineering*, Vol. 22, No. 2, 2009, pp. 173-184.
- [4] Stanford, B., “Aeroelastic Analysis and Optimization of Membrane Micro Air Vehicle Wings,” Ph.D. Dissertation, Department of Mechanical and Aerospace Engineering, University of Florida, Gainesville, FL, 2008.
- [5] Pornsin-sirirak, T., Tai, Y., Nassef, H., Ho, C., “Titanium-alloy MEMS Wing Technology for a Micro Aerial Vehicle Application,” *Sensors and Actuators A: Physical*, Vol. 89, No. 1-2, 2000, pp. 95-103.
- [6] Song, A., Tian, X., Israeli, E., Galvao, R., Bishop, K., Swartz, S., Breuer, K., “The Aero-Mechanics of Low Aspect Ratio Compliant Membrane Wings, with Applications to Animal Flight,” 46th AIAA Aerospace Sciences Meeting and Exhibit, Reno, NV, AIAA Paper 2008-517, 2008.
- [7] Leylek, E., Manzo, J., Garcia, E., “A Bat-wing Aircraft Using the Smart Joint Mechanism,” 3rd International Conference on Smart Materials, Structures, and Systems, Acireale, Sicily, 2008.
- [8] Manzo, J., Leylek, E., Garcia, E., “Drawing Insight from Nature: A Bat Wing for Morphing Aircraft,” ASME Conference on Smart Materials, Adaptive Structures, and Intelligent Systems, Ellicott City, MD, 2008.
- [9] Abdulrahim, M., Garcia, H., Lind, R., “Flight Characteristics of Shaping the Membrane Wing of a Micro Air Vehicle,” *Journal of Aircraft*, Vol. 42, No.1, 2005, pp. 131-137.
- [10] Waldman, R., Song, A., Riskin, D., Swartz, S., Breuer, K., “Aerodynamic Behavior of Compliant Membranes as Related to Bat Flight,” 38th Fluid Dynamics Conference and Exhibit, Seattle, WA, 2008.
- [11] Callahan, R., Garcia, E., “Bio-Inspired Bat Wing Design and Fabrication,” AIAA Region I-NE Student Conference, Worcester, MA, 2009.
- [12] Fink, J., *Reactive Polymers Fundamentals and Applications: A Concise Guide to Industrial Polymers*, William Andrew Publishing, Norwich, NY, 2005.

- [13] Keller, M., White, S., Sottos, N., “A Self-Healing Poly (Dimethyl Siloxane) Elastomer,” *Advanced Functional Materials*, Vol. 17, No. 14, 2007, pp. 2399-2404.
- [14] Boria, F., “Optimization of a Morphing Wing Geometry Using a Genetic Algorithm with Wind Tunnel Hardware-in-the-Loop,” M.S. Thesis, Department of Mechanical and Aerospace Engineering, University of Florida, Gainesville, FL, 2007.
- [15] Dally, J., Riley, W., *Experimental Stress Analysis*, College House Enterprises, Knoxville, TN, 2005.
- [16] Lee, K., “Development of Unmanned Aerial Vehicle (UAV) for Wildlife Surveillance,” M.S. Thesis, Department of Mechanical and Aerospace Engineering, University of Florida, Gainesville, FL, 2004.

BIOGRAPHICAL SKETCH

Albert Y. Lin was born in Taipei, Taiwan in 1980. His family moved to the United States in 1983, where his father attended graduate school at Auburn University. He later grew up in Tallahassee, Florida and graduated from Lincoln High School in 1999. Lin enrolled at the University of Florida later that year and received a Bachelor of Science in Aerospace Engineering in 2004. After graduating, he worked as an airborne LiDAR operator/analyst at the National Center for Airborne Laser Mapping (NCALM), conducting over 250 flight hours of aerial mapping across the United States in a Cessna 337 Skymaster. Lin joined the Micro Air Vehicle (MAV) Laboratory in 2007 with hopes of pursuing a graduate degree under the advisement of Dr. Peter Ifju. During this time, he was a member of a talented team of MAV researchers who designed a number of state-of-the-art aircraft. Lin received a Master of Science in Aerospace Engineering from the University of Florida in December 2009.